BACHELOR'S DEGREE THESIS

Degree in Mathematics

Title: Applications to Celestial Mechanics

Author: Adrià Torrent Canelles

Advisor: Mercè Ollé Torner

Department: Dept. de Matemàtiques

Academic year: 2017-18

UNIVERSITAT POLITÈCNICA DE CATALUNYA
BARCELONATECH
Facultat de Matemàtiques i Estadística

Acknowledgements

I would like to thank Mercè Oller Torner, my advisor, who has been essential during the whole project. All what you have taught to me and the passion and energy you have transmitted makes me very grateful.

Contents

1 Introduction **2**

2 The RTBP **3**
2.1 Equations of motion 3
2.2 Synodical coordinates 4
2.3 Equilibrium points of the RTBP 7
2.3.1 Equilibrium point L_1 8
2.3.2 Equilibrium point L_2 9
2.3.3 Equilibrium point L_3 9
2.4 Hill's regions 10
2.5 Levi-Civita regularization 11
2.5.1 Regularization around $(\mu, 0)$ 15
2.5.2 Regularization around $(\mu - 1, 0)$ 17

3 Periodic orbits around the equilibrium points **19**

4 Numerical simulations **22**
4.1 Computation procedure 23
4.2 Dynamical behavior of the invariant manifolds 25

5 Conclusions **39**

6 References **40**

7 Appendix **41**

1 Introduction

In this project we will deal with the Restricted Three Body Problem (RTBP) which is a simplification of the general problem of three bodies where we consider one of them with infinitessimal mass with respect to the other ones called primaries. Although the RTBP does not perfectly fit the real astrodynamics and celestial mechanics, it is very useful as a first insight and it is specially important due to the equilibrium points. There are a lot of applications related to them, such as studying the orbits of a spacecraft under the gravitational effect of the Earth-Moon system or the movement of Trojan asteroids in a neighbourhood of the triangular points of the Sun-Jupiter system. In 1978 the ISEE-3 became the first spacecreaft to fly on a libration point orbit (LPO) and from then on there have been several more missions, such as ACE, SOHO or WMAP. On the other hand, there exists an orbit around the equilibrium point L_2 in the Earth-Sun system which was proposed to place a space-based observatory with the goal to detect and analyze extrasolar planets similar to the Earth.

The richness of the dynamics of these points is given by the fact that they are center-center-saddle equilibrium points. This phenomenon gives rise to invariant unstable and stable manifolds of the equilibrium points which have been widely studied and there are many works related to them as for example Barrabés, Mondelo and Ollé [1]. On the other hand, also because of this property of the equilibrium points, there exist periodic orbits around each of them from which emanate invariant stable and unstable manifolds. Given these facts, our main goal in this project will be to study numerically the behavior of the invariant manifolds of the periodic orbits around the equilibrium points and understand how they depend on the mass parameter of the primaries and the orbit from where they start. Although we will explain how to compute the manifolds of the orbits around any of the collinear equilibrium points, we will only inspect numerically the orbits around the libration point L_1, which is placed between both primaries, and we will take a certain range of level of energy associated to the periodic orbit around it in order to focus on a single case as a first step for a possible further study considering the other equilibrium points and all the energy levels.

The project will be structured as follows. Section 2 states the conventions followed in the RTBP, the equations of the system, the computation of the equilibrium points of the problem, some important properties of the system and the Levi-Civita regularization around the primaries, basically based on the books Meyer, Hall and Offin [5], Stuart and Humphries [7] and Szebehely [8]. Section 3 gives the theoretical background to prove the existence of the periodic orbits around the equilibrium points and their manifolds, taking again as guide the results gathered in [5] and [8]. Finally in section 4 we develop all the numerical procedures used to compute the orbits and its invariant manifolds, explain the tools to describe their motion and show the results obtained from them.

2 The RTBP

In this section we will explain the basic concepts related to the RTBP. After considering the Newton's laws equations, we will deduct the synodical equations, which are the most commonly used when we deal with this problem. On the other hand, we will introduce the way how we compute the equilibrium points of the system and their positions on the (x, y) plane. Then we will work with Hill's region, which is a property of the problem that gives us the regions of the (x, y) plane where we can expect that each trajectory moves. Finally, we will introduce the Levi-Civita regularization, which is very important because it will allow us to integrate close to the primaries without having issues with the singularities caused by them.

2.1 Equations of motion

The three-body problem describes the motion of three bodies of mass m_1, m_2 and m_3 which are under their mutual gravitational attraction. In a reference frame such that the origin point is the center of mass of the system, which is fixed, the movement equations are

$$\begin{cases} \ddot{\vec{r}}_1 = \dfrac{Gm_2}{r_{12}^3}(\vec{r}_2 - \vec{r}_1) + \dfrac{Gm_3}{r_{13}^3}(\vec{r}_3 - \vec{r}_1) \\ \ddot{\vec{r}}_2 = \dfrac{Gm_1}{r_{12}^3}(\vec{r}_1 - \vec{r}_2) + \dfrac{Gm_3}{r_{23}^3}(\vec{r}_3 - \vec{r}_3) \\ \ddot{\vec{r}}_3 = \dfrac{Gm_1}{r_{13}^3}(\vec{r}_1 - \vec{r}_3) + \dfrac{Gm_2}{r_{23}^3}(\vec{r}_2 - \vec{r}_3) \end{cases} \tag{2.1}$$

where G is the gravitational constant and $\vec{r}_1$, $\vec{r}_2$, $\vec{r}_3 \in \mathbb{R}^3$ are the positions of each body and $r_{ij} = ||\vec{r}_i - \vec{r}_j||$ are the distances between them.

In our case, we only focus on the Restricted Three Body Problem (RTBP), where we consider two massive bodies, the primaries, and a third one which has an infinitessimal mass in comparison with the other ones. Considering m_1 and m_2 the masses of the primaries, then our movement equations are

$$\begin{cases} \ddot{\vec{r}}_1 = \dfrac{Gm_2}{r_{12}^3}(\vec{r}_2 - \vec{r}_1) \\ \ddot{\vec{r}}_2 = \dfrac{Gm_1}{r_{12}^3}(\vec{r}_1 - \vec{r}_2) \\ \ddot{\vec{r}}_3 = \dfrac{Gm_1}{r_{13}^3}(\vec{r}_1 - \vec{r}_3) + \dfrac{Gm_2}{r_{23}^3}(\vec{r}_2 - \vec{r}_3) \end{cases} \tag{2.2}$$

so the third body does not affect on the primaries' movement. We do two additional assumptions, which are that the primaries perform a circular orbit and that the third body follows an orbit contained in plane of rotation of the primaries, giving rise to the Restricted Circular Planar Three Body Problem (RCPTBP).

2.2 Synodical coordinates

As the third body's motion is explained by

$$\ddot{\vec{r}}_3 = \frac{Gm_1}{r_{13}^3}(\vec{r}_1 - \vec{r}_3) + \frac{Gm_2}{r_{23}^3}(\vec{r}_2 - \vec{r}_3) \tag{2.3}$$

we separate $\vec{r}_3 = (X, Y)$, hence:

$$\begin{cases} \ddot{X} = -Gm_1\dfrac{X - X_1}{R_1^3} - Gm_2\dfrac{X - X_2}{R_2^3} \\ \ddot{Y} = -Gm_1\dfrac{Y - Y_1}{R_1^3} - Gm_2\dfrac{Y - Y_2}{R_2^3} \end{cases} \tag{2.4}$$

where $R_1 = \sqrt{(X - X_1)^2 + (Y - Y_1)}$ and $R_2 = \sqrt{(X - X_2)^2 + (Y - Y_2)^2}$. Given the fact that the primaries are rotating following a circular orbit, let's call n their angular velocity and ρ_1 and ρ_2 their respective orbit radius (where $\rho_1 + \rho_2 = l$) and consider $M = m_1 + m_2$. Hence we have that

$$\begin{cases} X_1 = \rho_1 cos(nt) & Y_1 = \rho_2 sin(nt) \\ X_2 = -\rho_2 cos(nt) & Y_2 = -\rho_2 sin(nt) \end{cases}$$

Considering complex numbers it it easier. Hence define $Z = X + iY$ and $z = x + iy$, where the last ones are the new variables we are going to use. Then we have $Z = ze^{nti}$, $Z_1 = \rho_1 e^{nti}$ and $Z_2 = -\rho_2 e^{nti}$ so we finally have

$$\begin{cases} R_1 = \sqrt{(X - X_1)^2 + (Y - Y_1)^2} = |ze^{nti} - \rho_1 e^{nti}| = |z - \rho_1| = \sqrt{(x - \rho_1)^2 + y^2} \\ \\ R_2 = \sqrt{(X - X_2)^2 + (Y - Y_2)^2} = |ze^{nti} + \rho_2 e^{nti}| = |z + \rho_2| = \sqrt{(x + \rho_2)^2 + y^2} \end{cases}$$

We can also compute the equation (2.4) with complex variables, so on the left hand side we have

$$\dot{Z} = \dot{z}e^{nti} + inze^{nti} \Longrightarrow \ddot{Z} = (\ddot{z} + 2in\dot{z} - n^2 z)$$

and on the right hand side

$$-G\Big[m_1\frac{z - \rho_1}{|z - \rho_1|} + m_2\frac{z + \rho_2}{|z + \rho_2|}\Big].$$

so we finally have

$$\ddot{z} + 2in\dot{z} - n^2 z = -G\left[m_1\frac{z - \rho_1}{|z - \rho_1|} + m_2\frac{z + \rho_2}{|z + \rho_2|}\right] \tag{2.5}$$

We can separate the real and the imaginary part giving rise to the following equations

$$\begin{aligned} \ddot{x} - 2n\dot{y} - n^2 x &= -G\left[m_1\frac{x - \rho_1}{((x - \rho_1)^2 + y^2)^{3/2}} + m_2\frac{x + \rho_2}{((x + \rho_2)^2 + y^2)^{3/2}}\right] \\ \ddot{y} + 2n\dot{x} - n^2 y &= -G\left[m_1\frac{y}{((x - \rho_1)^2 + y^2)^{3/2}} + m_2\frac{y}{((x + \rho_2)^2 + y^2)^{3/2}}\right] \end{aligned} \tag{2.6}$$

or equivalently

$$\begin{aligned} \ddot{x} - 2n\dot{y} - n^2 x &= -G\left[m_1 \frac{x-\rho_1}{r_1^3} + m_2 \frac{x+\rho_2}{r_2^3}\right] \\ \ddot{y} + 2n\dot{x} - n^2 y &= -G\left[m_1 \frac{y}{r_1^3} + m_2 \frac{y}{r_2^3}\right] \end{aligned} \tag{2.7}$$

Let us define a very useful function that will simplify our equations:

$$F = \frac{n^2}{2}(\dot{x}^2 + \dot{y}^2) + G\Big(\frac{m1}{r1} + \frac{m2}{r2}\Big)$$

and differentiating

$$\frac{\partial F}{\partial x} = n^2 x - G\Big[m_1 \frac{x-\rho_1}{r_1^3} + m_2 \frac{x+\rho_2}{r_2^3}\Big]$$

$$\frac{\partial F}{\partial y} = n^2 y - G\Big[m_1 \frac{y}{r_1^3} + m_2 \frac{y}{r_2^3}\Big]$$

so we can write the equation (2.5) as

$$\begin{cases} \ddot{x} - 2n\dot{y} = \dfrac{\partial F}{\partial x} \\ \ddot{y} + 2n\dot{x} = \dfrac{\partial F}{\partial y} \end{cases} \tag{2.8}$$

Taking these two equations and multiplying the first one by $\dot{x}$, the second one by $\dot{y}$ and adding both we get

$$\dot{x}\ddot{x} + \dot{y}\ddot{y} = \frac{\partial F}{\partial x}\dot{x} + \frac{\partial F}{\partial y}\dot{y} = \frac{dF}{dt}$$

integrating

$$\frac{1}{2}\dot{x}^2 + \frac{1}{2}\dot{y}^2 = F - \frac{C*}{2}$$

where $C*$ is an arbitrary constant, which is known as the Jacobi integral. These equations are also converted to dimensionless ones, so we do a change of variables as follows

$$\xi = \frac{x}{l},\ \eta = \frac{y}{l},\ \tau = nt,\ r_1 = \frac{R_1}{l},\ r_2 = \frac{R_2}{l},\ \mu_1 = \frac{m_1}{M},\ \mu_2 = \frac{m_2}{M}$$

and then we obtain

$$\begin{cases} \ddot{\xi} - 2\dot{\eta} = \bar{\Omega}_\xi \\ \ddot{\eta} + 2\dot{\xi} = \bar{\Omega}_\eta \end{cases} \tag{2.9}$$

where the function $\bar{\Omega}$ is

$$\bar{\Omega} = \frac{F}{n^2 l^2} = \frac{1}{2}(\xi^2 + \eta^2) + \frac{\mu_1}{r_1} + \frac{\mu_2}{r_2}$$

There is a convention to add $\bar{\Omega}$ a constant to make this expression more symmetric

$$\Omega = \bar{\Omega} + \frac{1}{2}\mu_1\mu_2$$

Taking into account that in these dimensionless variables we have that $r_1^2 = (\xi - \rho_1)^2 + \eta^2$ and $r_2^2 = (\xi + \rho_2)^2 + \eta^2$, then we get

$$\Omega = \frac{1}{2}\Big[\mu_1 r_1^2 + \mu_2 r_2^2 + \frac{\mu_1}{r_1} + \frac{\mu_2}{r_2}\Big]$$

Differentiating this expression we get

$$\Omega_\xi = \xi - \frac{\mu_1(\xi - \mu_1)}{r_1^3} - \frac{\mu_2(\xi + \mu_2)}{r_2^3}$$
$$\Omega_\eta = \eta\Big[1 - \frac{\mu_1}{r_1^3} - \frac{\mu_2}{r_2^3}\Big]$$

So finally we have the equations

$$\begin{cases} \ddot{\xi} - 2\dot{\eta} = \Omega_\xi \\ \ddot{\eta} + 2\dot{\xi} = \Omega_\eta \end{cases} \tag{2.10}$$

With all these changes the new Jacobi integral is

$$C = \frac{C*}{n^2 l^2} + \frac{1}{2}\mu_1\mu_2 = 2\Omega(\xi, \eta) - \dot{\xi}^2 - \dot{\eta}^2.$$

From now on we assume that $\mu_1 + \mu_2 = 1$, so we can write them as $\mu_1 = 1 - \mu$ and $\mu_2 = \mu$ where $\mu \in [0, 0.5]$. By doing so the massive body is on the right of the center of gravity and their positions are μ_1 at $(\mu, 0)$ and μ_2 at $(\mu - 1, 0)$. Just to use the typical notation we call x and y the new variables instead of ξ and η. Summarizing our results, the equations of motion of the third body are

$$\begin{cases} \ddot{x} - 2\dot{y} = \Omega_x \\ \ddot{y} + 2\dot{x} = \Omega_y \end{cases} \tag{2.11}$$

where the function Ω is

$$\Omega = \frac{1}{2}\Big[(1 - \mu)r_1^2 + \mu r_2^2 + \frac{1 - \mu}{r_1} + \frac{\mu}{r_2}\Big]$$

and the distances to both primaries are $r_1 = \sqrt{(x - \mu)^2 + y^2}$ and $r_2 = \sqrt{(x - \mu + 1)^2 + y^2}$. In addition, we have the Jacobi integral

$$C = 2\Omega(x, y) - \dot{x}^2 - \dot{y}^2 \tag{2.12}$$

which is a very useful property when integrating numerically trajectories of the third body because we can see if it is following properly the trajectory by checking that this value remains constant.

Furthermore, it is important to keep in mind a very useful property of the problem, which is the well known symmetry

$$(x, y, \dot{x}, \dot{y}, t) \longrightarrow (x, -y, -\dot{x}, \dot{y}, -t). \tag{2.13}$$

This implies that for each solution of the equation (2.11), there also exists another one, which is seen to be symmetric with respect to $y = 0$ in configuration space. This symmetry can be easily proved by simply assuming that $(x, y, \dot{x}, \dot{y})$ is a solution and then substituting the symmetric values in the synodical equations we get that it is also a solution of the system.

2.3 Equilibrium points of the RTBP

Taking the equations of motion in synodical coordinates, we have:

$$\begin{cases} \ddot{x} - 2\dot{y} = \Omega_x \\ \ddot{y} + 2\dot{x} = \Omega_y \end{cases}$$

Doing a simple change of variable such that $y_1 = x$, $y_2 = y$, $y_3 = \dot{x}$ and $y_4 = \dot{y}$, we get a first order ODE system as follows:

$$\begin{cases} \dot{y_1} = y_3 \\ \dot{y_2} = y_4 \\ \dot{y_3} = 2\dot{y_2} + \Omega_{y_1} \\ \dot{y_4} = -2\dot{y_1} + \Omega_{y_2} \end{cases}$$

Our goal in this section is to compute the different equilibrium points of the RTBP, which is equivalent to require that $\dot{x} = \dot{y} = 0$ and

$$\begin{cases} \Omega_{y_1} = 0 \\ \Omega_{y_2} = 0 \end{cases}$$

Using again the $(x, y, \dot{x}, \dot{y})$ notation, we then have

$$\begin{cases} \Omega_x = 0 \\ \Omega_y = 0 \end{cases} \iff \begin{cases} x - \dfrac{(1-\mu)(x-\mu)}{r_1^3} - \dfrac{\mu(x+1-\mu)}{r_2^3} = 0 \\ y\Big(1 - \dfrac{1-\mu}{r_1^3} - \dfrac{\mu}{r_2^3}\Big) = 0 \end{cases}$$

Where $r_1 = \sqrt{(x-\mu)^2 + y^2}$ and $r_2 = \sqrt{(x-\mu+1)^2 + y^2}$ are the distances to both massive bodies. As we see in the second equation, we can differentiate between two cases depending on the value of y:

- If $y = 0$: these are the collinear equilibrium points L_1, L_2 and L_3, which are aligned with the two primaries.
- If $y \neq 0$: these are the values associated to the points L_4 and L_5. In this it is well known that these points are symmetric with respect to the x-axis and are placed at $(\mu - 1/2, \pm\sqrt{3}/2)$, see Szebehely [8].

In figure (2.1) we plot the location of L_i, $i = 1, ..., 5$ on the (x, y) plane for $\mu = 0.2$.

From now on we will only take into account the collinear equilibrium points. As usual, we consider L_1, L_2 and L_3 such that $x_{L_2} < \mu - 1 < x_{L_1} < \mu < x_{L_3}$. Before explaining how to compute them, we may introduce a very useful theorem for our purpose:

Theorem 2.1 (Descartes' Theorem)**.** *Given a polynomial $a_0x^n + \cdots + a_{n-1}x + a_n$, the number of positive roots is less or equal to the number of changes of sign of the coefficients $a_0, \ldots, a_n$.*

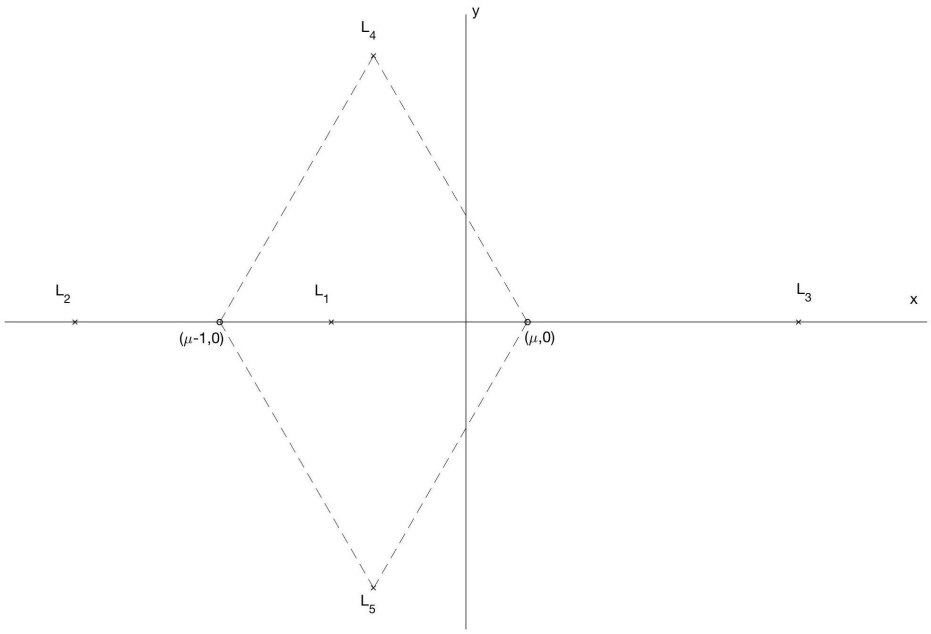

Figure 2.1: Position of the equilibrium points and the primaries on the (x, y) plane for $\mu = 0.2$

2.3.1 Equilibrium point L_1

As $y = 0$, it's accomplished that $\Omega_y = 0$, so we only need to focus on the first equation. As $\mu - 1 < x_{L_1} < \mu$, we can use $x = \mu - 1 + \xi_{L_1}$ where $\xi_{L_1} \in (0, 1)$. Using that $r_1 = 1 - \xi_{L_1}$ and $r_2 = \xi_{L_1}$, we get

$$\Omega_x(x_{L_1}, 0) = 0 \Longleftrightarrow \mu - 1 + \xi_{L_1} - \frac{1-\mu}{(1-\xi_{L_1})^2} - \frac{\mu}{\xi_{L_1}^2} \Longleftrightarrow \xi_{L_1}^5 - (3-\mu)\xi_{L_1}^4 + (3-2\mu)\xi_{L_1}^3 - \mu\xi_{L_1}^2 + 2\mu\xi_{L_1} - \mu = 0$$

which is the so called Euler quintic polynomial equation. Notice that in the last step we have multiplied the whole equation by $\xi_{L_1}^2(1-\xi_{L_1})^2$. If we call the last polynomial as $P_1(\xi)$, we then have that $P_1(0) = -\mu < 0$ and $P_1(1) = 1 - \mu > 0$, so at least there exists a root of this polynomial in the interval $(0, 1)$ because of Bolzano's theorem. In addition, $P_1'(\xi) > 0 \ \forall \xi \in (0, 1)$, so we arrive to the conclusion that $\exists! \xi_{L_1} \in (0, 1)$ such that $P_1(\xi_{L_1}) = 0$. Instead of trying to find the zero of this polynomial, we can handle its expression in order to reach the following expression:

$$\xi = \Big(\frac{\mu(1-\xi)^2}{3 - 2\mu - \xi(3-\mu-\xi)}\Big)^{1/3} =: f_1(\xi)$$

So we have changed our goal from finding the zero of $P_1(\xi)$ to finding a fix point $f_1(\xi)$. Using as first approximation $\xi_0 = \Big(\frac{\mu}{3(1-\mu)}\Big)^{1/3}$, see Szebehely [8], we will be able to find the fix point by defining a succession of values $(\xi_n)_{n\in\mathbb{N}}$ such that $\xi_i = f_1(\xi_{i-1})$ for $i > 0$ and we compute until we reach $|\xi_i - f_1(\xi_{i-1})| < \varepsilon$, where ε is a the tolerance required.

2.3.2 Equilibrium point L_2

Using the same reasoning as before, $x_{L_2} < \mu - 1$ so we have $x_{L_2} = \mu - 1 - \xi_2$ where $\xi_2 \in (0, \infty)$. Using this notation we have that $r_1 = 1 + \xi_2$ and $r_2 = \xi_2$, so we have:

$$\Omega_x(x_{L_2}, 0) = 0 \Longleftrightarrow \mu - 1 - \xi_{L_2} - \frac{1-\mu}{(-1+\xi_{L_2})^2} - \frac{\mu}{\xi_{L_2}^2} \Longleftrightarrow \xi_{L_2}^5 + (3-\mu)\xi_{L_2}^4 + (3-2\mu)\xi_{L_2}^3 - \mu\xi_{L_2}^2 - 2\mu\xi_{L_2} - \mu = 0$$

Calling $P_2(\xi)$ the last polynomial, we have that $P_2(0) = -\mu < 0$ and $P_2(1) = 7 - 7\mu > 0$ so as before we have at least a root of P_2 in the interval $(0, 1)$. If we take into account the Descartes' theorem, we then have that there is a single change of sign so eventually we only have a positive root of the polynomial, which belongs to the previous interval. Again, we can manipulate the polynomial expression so we get the following equality:

$$\xi = \Big(\frac{\mu(1+\xi)^2}{3 - 2\mu + \xi(3 - \mu + \xi)}\Big)^{1/3} =: f_2(\xi)$$

After this transformation, we have another fix point problem to be solved the same way as before and in this case we use the same initial approximation $\xi_0 = \Big(\frac{\mu}{3(1-\mu)}\Big)^{1/3}$.

2.3.3 Equilibrium point L_3

The last equilibrium point to be computed is L_3, the one placed at $x_{L_3} > \mu$, so we define it as $x_{L_3} = \mu + \xi_{L_3}$, so $r_1 = \xi_{L_3}$ and $r_2 = 1 + \xi_{L_3}$. Then we have:

$$\Omega_x(x_{L_3}, 0) = 0 \Longleftrightarrow \mu - 1 - \xi_{L_3} - \frac{1-\mu}{(-1+\xi_{L_3})^2} - \frac{\mu}{\xi_{L_3}^2} \Longleftrightarrow$$

$$\Longleftrightarrow \xi_{L_3}^5 + (2+\mu)\xi_{L_3}^4 + (1+2\mu)\xi_{L_3}^3 - (1-\mu)\xi_{L_3}^2 - 2(1-\mu)\xi_{L_3} - (1-\mu) = 0$$

This last polynomial is called from now on as $P_3(\xi)$, which accomplishes that $P_3(0) = -1 + \mu < 0$ and $P_3(1) = 7\mu > 0$ so we have (at least) a root of this polynomial in the interval $(0, 1)$. In addition, because of the Descartes' theorem we have that there is at most one positive root of the polynomial, so we eventually conclude that $\exists! \xi_{L_3} \in (0, 1)$ such that $P_3(\xi_{L_3}) = 0$. After a little manipulation, we get the following equivalent expression:

$$\xi = \Big(\frac{(1-\mu)(1+\xi)^2}{1 + 2\mu + \xi(2 + \mu + \xi)}\Big)^{1/3} =: f_3(\xi)$$

Hence, we need to find the fix point of the function $f_3(\xi)$ in order to compute the equilibrium point L_3 and we take as initial value $\xi_0 = 1 - \frac{7}{12}\mu$, see Szebehely [8], and do the same procedure that we have already seen with the previous equilibrium points.

Finally we provide in figure (2.2) the x coordinate of L_i, $i = 1, 2, 3$, depending on $\mu \in (0, 1/2]$ and the corresponding values of the Jacobi integral $C_i = C(L_i)$, $i = 1, 2, 3$.

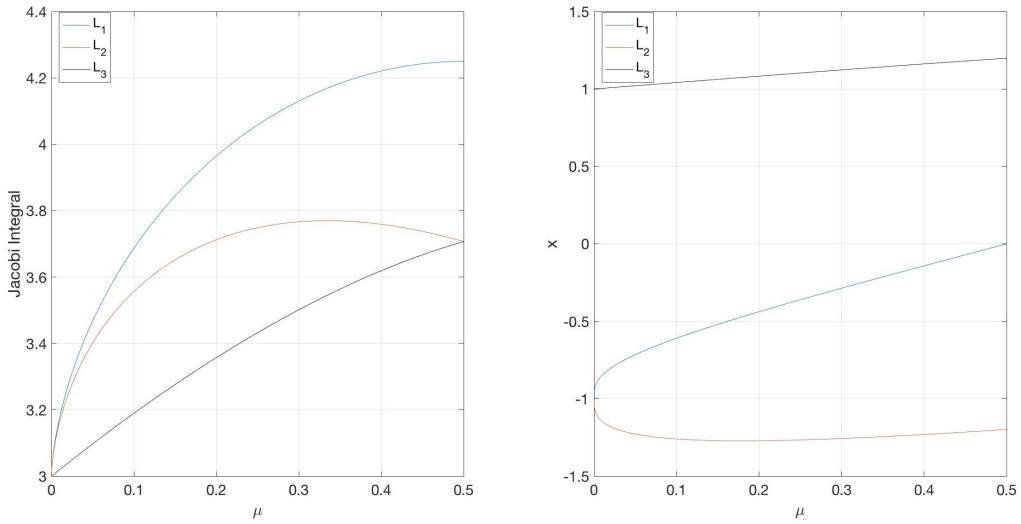

Figure 2.2: Jacobi integral and x coordinate of the equilibrium points depending on μ.

2.4 Hill's regions

The RTBP has another important property: Hill's regions. Taking a look to the expression of the Jacobi integral we have that

$$2\Omega(x,y) - C = \dot{x}^2 + \dot{y}^2 \geq 0 \tag{2.14}$$

Hence, for a certain level C we can define the Hill's region as

$$R(C) = \{(x,y) \in \mathbb{R}^2 \mid 2\Omega(x,y) \geq C\} \tag{2.15}$$

and the boundary of $R(C)$ which is $2\Omega(x,y) = C$ (equivalently $\dot{x} = \dot{y} = 0$) is called the zero velocity curve. This property implies that for given initial condition $(x_0, y_0, \dot{x}_0, \dot{y}_0)$ with Jacobi integral C, we know that whatever the trajectory does, it will never cross the boundary of Hill's region $R(C)$.

Defining $C_i = C(L_i)$, $i = 1, ..., 5$, we plot it in figure (2.3) the Hill's region for a given value μ for values of C greater than C_2, which are the values that we want to study. We remark how the topology of the regions changes whenever C crosses a value C_i, $i = 1, ..., 5$.

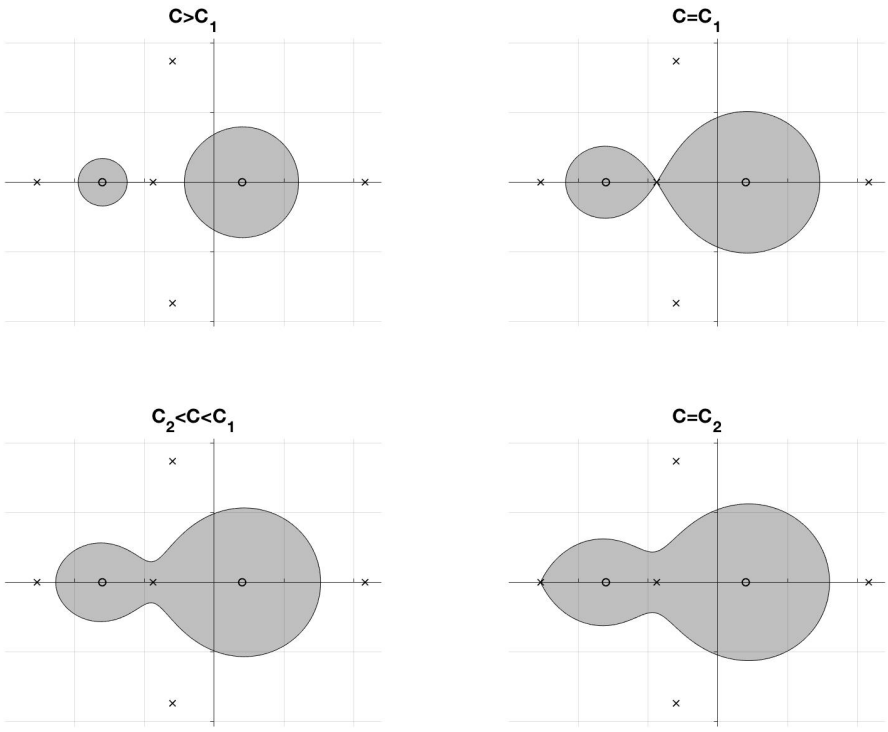

Figure 2.3: Hill's region for different values of $C \geq C_2$. The shaded area is the permitted one, the rounded points locate the primaries and the cross points the equilibrium points.

2.5 Levi-Civita regularization

The synodical coordinates are the most natural ones when trying to understand the dynamics behind the equations as they do not involve nothing but basically fixing a rotating reference system and proportional magnitudes from the Newton equations. The main problem of the synodical coordinates is that there appear two singularities at $(\mu, 0)$ and $(\mu - 1, 0)$. This implies that it is impossible to inspect numerically when we are close to these points because our methods would not be accurate, so we must find a way to compute the solutions of the system in a neighbourhood of the primaries without losing accuracy.

A possible solution is considering the Levi-Civita regularization, which consist of a regularization for each of the primaries such that we avoid its singularity and there only exists a singularity in the transformed system of ODE which is placed at the other primary. Taking the expression of the

RTBP in synodical coordinates we have:

$$\begin{cases} \ddot{x} - 2\dot{y} = \Omega_x \\ \ddot{y} + 2\dot{x} = \Omega_y \end{cases} \iff \ddot{z} + 2i\dot{z} = grad_z\Omega \tag{2.16}$$

where $\dot{z} = \dfrac{dz}{dt}$, $z = x + iy$ and $grad_z\Omega = \Omega_x + i\Omega_y$. Because of the definition of Ω, if $r_1 \longrightarrow 0$ or $r_2 \longrightarrow 0$ then the equations become singular (there is a collision with either of the primaries). So the goal of this section is to find a regularization of these equations such that we avoid these singularities. Hence, we consider two transformations

$$\begin{cases} z = f(w) \\ \dfrac{dt}{ds} = g(w) = |f'(w)|^2 \end{cases} \tag{2.17}$$

where $w = u + iv$. We must notice that this transformation involves both time and position. Before arriving to our equations, we must introduce a proposition which needs some lemmas to be proved.

Proposition 2.1. *(i) The equation (2.16), after the transformation (2.17), becomes*

$$w'' + 2i|f'|^2 w' = |f'|^2 grad_w\tilde{\Omega} + \frac{|w'|^2\overline{f}''}{\overline{f}'}$$

with $\Omega(x, y) = \Omega(x(u, v), y(u, v)) = \tilde{\Omega}(u, v)$.

(ii) Defining $\mathcal{U} = \tilde{\Omega} - \frac{C}{2}$ *and using that* $C = 2\Omega(x, y) - (\dot{x}^2 + \dot{y}^2)$ *we obtain*

$$w'' + 2i|f'|^2 w' = grad_w(\mathcal{U}|f'|^2)$$

Proof.

$$\dot{z} = \frac{dz}{dw}\frac{dw}{ds}\frac{ds}{dt} = f'w'\dot{s}$$

$$\ddot{z} = f'w'\ddot{s} + f''w'\dot{s}w'\dot{s} + f'w''\dot{s}^2 = f'w'\ddot{s} + (f''w'^2 + f'w'')\dot{s}^2$$

Let us transform $grad_z\Omega$.

Lemma 2.1.

$$\overline{f}' grad_z\Omega = grad_w\tilde{\Omega}$$

where $grad_w\tilde{\Omega} = \tilde{\Omega}_u + i\tilde{\Omega}_v$

Proof.

$$z = x + iy = f(w) = f(u, v) \Longrightarrow \frac{df}{dw} = \frac{\partial f}{\partial u} = x_u + iy_u = -\frac{\partial f}{\partial v}$$

From Cauchy-Riemann equations we know that $x_u = y_v$ and $x_v = -y_v$ so we have

$$grad_w\tilde{\Omega} = \tilde{\Omega}_u + i\tilde{\Omega}_v = \Omega_x x_u + \Omega_y y_u + i(\Omega_x x_v + \Omega_y y_v) = \Omega_x x_u + \Omega_y y_u + i(-\Omega_x y_u + \Omega_y x_u) =$$

$$= (x_u - iy_u)(\Omega_x + i\Omega_y) = \overline{f}' grad_z\Omega$$

□

Hence, equation (2.16) reads

$$f'w'\ddot{s} + (f'w'' + f''w'^2)\dot{s}^2 + 2if'w'\dot{s} = \frac{1}{\overline{f}'}grad_w\tilde{\Omega}$$

Dividing by $f'\dot{s}^2$ and placing each term properly, we obtain

$$w'' + w'\frac{\ddot{s}}{\dot{s}^2} + i\frac{2w'}{\dot{s}} = -\frac{w'^2f''}{f'} + \frac{1}{|f'|^2\dot{s}^2}grad_w\tilde{\Omega} \tag{2.18}$$

Let us compute $\frac{\ddot{s}}{\dot{s}^2}$:

$$\left.\begin{aligned} \dot{s} = \frac{1}{g} = \frac{1}{|f'|^2} = \frac{1}{f'\overline{f'}} \\ \ddot{s} = -\frac{\dot{g}}{g^2} = -\dot{g}\dot{s}^2 \end{aligned}\right\} \Longleftrightarrow \frac{\ddot{s}}{\dot{s}^2} = -\dot{g}$$

Lemma 2.2.

$$\dot{g} = \frac{\overline{f}''\overline{w}'}{\overline{f}'} + \frac{f''w'}{f'}$$

Proof.

$$\dot{g} = f'\frac{d\overline{f}'}{dt} + \overline{f}'\frac{df'}{dt} = (f'\overline{f}''\overline{w}' + \overline{f}'f''w')\dot{s} = \frac{\overline{f}''\overline{w}'}{\overline{f}'} + \frac{f''w'}{f'}$$

where in the first equality we have used that

$$\frac{df'}{dt} = \frac{df'}{dw}\frac{dw}{ds}\frac{ds}{dt} = f''w'\dot{s}$$

$$\frac{d\overline{f}'}{dt} = \overline{\frac{df}{dt}} = \overline{\frac{df'}{dw}}\,\overline{\frac{dw}{ds}}\frac{ds}{dt} = \overline{f}''\overline{w}'\dot{s}$$

while in the second one we use that $\dot{s} = \frac{1}{f'\overline{f}'}$. □

So equation (2.18) becomes

$$w'' - w'\Big(\frac{\overline{f}''\overline{w}'}{\overline{f}'} + \frac{f''w'}{f'}\Big) + 2i|f'|^2w' = -\frac{w'^2f''}{f'} + |f'|^2grad_w\tilde{\Omega}$$

or equivalently

$$w'' + 2i|f'|^2w' = |f'|^2grad_w\tilde{\Omega} + \frac{|w'|^2\overline{f}''}{\overline{f}'} =: RT \tag{2.19}$$

as (i) proves. Let us focus now on the second part of the proposition. We use $U = \tilde{\Omega} - \frac{C}{2}$ so $grad_w\tilde{\Omega} = grad_wU$. Then, from the Jacobi integral

$$|\dot{z}|^2 = 2\tilde{\Omega} - C = 2U \Longleftrightarrow 2U = |f'|^2|w'|^2\dot{s}^2 = \frac{|w'|^2}{|f'|^2} \Longleftrightarrow |w'|^2 = 2|f'|^2U$$

So

$$RT = |f'|^2 grad_w U + \frac{2|f'|^2 U \overline{f}''}{\overline{f}'} = |f'|^2 grad_w U + 2f'\overline{f}'' U$$

Now we use the following lemma

Lemma 2.3. *If $g_1(w)$, $g_2(w)$ are real analytic functions of a complex variable w, then:*

1. $grad_w(g_1 g_2) = g_1 grad_w g_2 + g_2 grad_w g_1$
2. *If $G(w)$ is an analytic complex function of a complex variable, then* $grad_w|G(w)|^2| = 2G\overline{\frac{dG}{dw}}$

Proof. 1.

$$grad_w(g_1 g_2) = (g_1 g_2)_v + i(g_1 g_2)_v = g_{1_u} g_2 + g_1 g_{2_u} + i g_{1_v} g_2 + i g_1 g_{2_v} =$$

$$= g_1(g_{2_u} + i g_{2_v}) + g_2(g_{1_u} + i g_{1_v}) = g_1 grad_w g_2 + g_2 grad_w g_1$$

2. Calling $G = R + iI$ then we have

$$|G|^2 = R^2 + I^2 \Longrightarrow grad_w|G|^2 = 2RR_u + 2II_u + i(2RR_v + 2II_v)$$

$$2G\overline{\frac{dG}{dw}} = 2(R+iI)(R_u - iI_u) = 2[RR_u + II_u + i(-RI_u + IR_u)] = grad_w|G|^2$$

where in the last equality we use Cauchy-Riemann ($R_u = I_v$, $R_v = -I_u$).

□

Therefore,

$$grad_w(U|f'|^2) = U grad_w(|f'|^2) + |f'|^2 grad_w U = U 2f'\overline{f}'' + |f'|^2 grad_w U = RT$$

where in the first equality we have used the first part of the lemma and in the second equality the second part. So finally we have reached our goal because

$$w'' + 2i|f'|^2 w' = grad_w(U|f'|^2)$$

and the proposition is proved. □

When working with the RTBP we must consider the singularities at $(\mu, 0)$ and $(\mu - 1, 0)$, which are the position of the primaries, so we will consider a transformation for each of them:

(a) For $(\mu, 0)$ we take $z = f(w) = \mu + w^2$

(b) For $(\mu - 1, 0)$ we take $z = f(w) = \mu - 1 + w^2$

where $z = x + iy$ and $w = u + iv$. So in both cases we have $\frac{dt}{ds} = |f'(w)|^2 = 4(u^2 + v^2)$. These transformations will give us the Levi-Civita equations. Hence, using the previous proposition and these functions, we have in both cases that the movement equations are

$$u'' + iv'' + 8i(u^2 + v^2)(u' + iv') = (4U(u^2 + v^2))_u + i(4U(u^2 + v^2))_v \Longleftrightarrow$$

$$\iff \begin{cases} u'' - 8(u^2+v^2)v' = (4U(u^2+v^2))_u \\ v'' + 8(u^2+v^2)u' = (4U(u^2+v^2))_v \end{cases}$$

So we only have to take into account that in each case the expression of U is different and that the equivalence of the w-coordinates with the z-coordinates are not the same. It is also remarkable that U depends on the Jacobi integral.

As we re-scale the time, we must take into account the change of variables of the velocities

$$\dot{z} = \frac{dz}{dt} = \frac{d}{dt}(f(w)) = \frac{df}{dw}\frac{dw}{ds}\frac{ds}{dt} = \frac{2ww'}{4(u^2+v^2)} = \frac{uu'-vv'}{2(u^2+v^2)} + i\frac{uv'+vu'}{2(u^2+v^2)} \iff \begin{cases} \frac{dx}{dt} = \frac{uu'-vv'}{2(u^2+v^2)} \\ \frac{dy}{dt} = \frac{uv'+vu'}{2(u^2+v^2)} \end{cases}$$

On the other hand, if we want to do the inverse change

$$\begin{cases} \dot{x} = \frac{uu'-vv'}{2(u^2+v^2)} \\ \dot{y} = \frac{uv'+vu'}{2(u^2+v^2)} \end{cases} \iff \begin{cases} 2\dot{x}(u^2+v^2) = uu'-vv' \\ 2\dot{y}(u^2+v^2) = uv'+vu' \end{cases} \iff$$

$$\iff \begin{cases} 2(u^2+v^2)(\dot{x}u+\dot{y}v) = (u^2+v^2)u' \\ 2(u^2+v^2)(-\dot{x}v+\dot{y}u) = (u^2+v^2)v' \end{cases} \iff \begin{cases} u' = 2(\dot{x}u+\dot{y}v) \\ v' = 2(-\dot{x}v+\dot{y}u) \end{cases}$$

where both u and v depend on the primary around which we are.

2.5.1 Regularization around $(\mu, 0)$

As we have already said, we consider $z = f(w) = \mu + w^2$ and $\frac{dt}{ds} = 4(u^2+v^2)$, where $z = x+iy$ and $w = u+iv$. Hence we have

$$\begin{cases} x = \mu + u^2 - v^2 \\ y = 2uv \\ \dot{x} = \frac{uu'-vv'}{2(u^2+v^2)} \\ \dot{y} = \frac{uv'+vu'}{2(u^2+v^2)} \end{cases} \iff \begin{cases} u = \pm\sqrt{\frac{x-\mu+\sqrt{(x-\mu)^2+y^2}}{2}} \\ v = \pm\sqrt{-x+\mu+u^2} \\ u' = 2(\dot{x}u+\dot{y}v) \\ v' = 2(-\dot{x}v+\dot{y}u) \end{cases}$$

Using this change of variables, the new coordinates of the primaries and the origin point are

$$\begin{cases} z_1 = \mu \longrightarrow w_1 = 0 \\ z_2 = \mu - 1 \longrightarrow w_2 = \pm i \\ O_z = 0 \longrightarrow O_w = \pm i\sqrt{\mu} \end{cases}$$

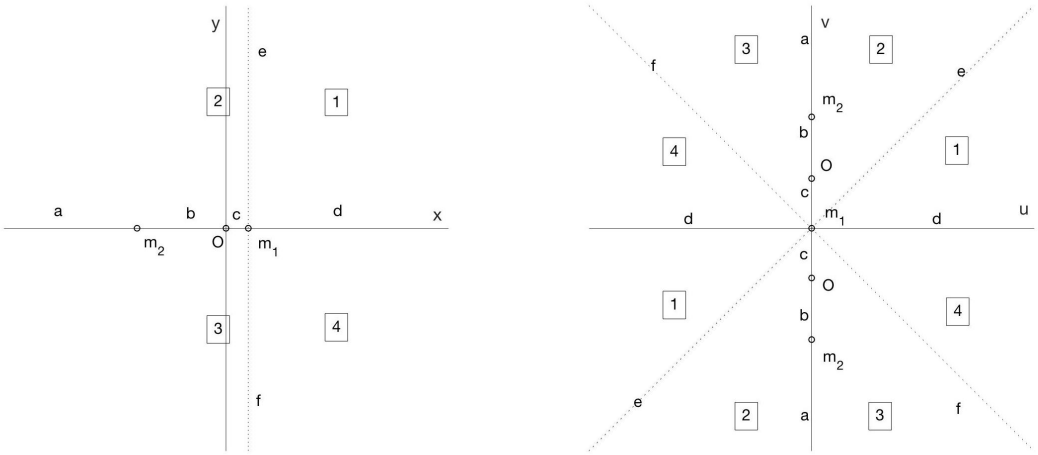

Figure 2.4: Representation of the change of variables from synodical coordinates on the (x, y) plane (left) and Levi-Civita coordinates around m_1 on the (u, v) plane (right). The point called O is the origin point in synodical coordinates while m_1 and m_2 correspond to the primaries. Characters a-f represent the segments of the x-axis or the vertical line $\{x = \mu\}$. On the other hand, sectors 1-4 make reference to the regions delimited by the x-axis and $\{x = \mu\}$ (left) or the regions delimited by the diagonals and the axis (right).

In figure (2.4) we represent the transformation between both system of coordinates and we can understand more properly how each region of the plane (x, y) is transformed in the (u, v) plane. We must notice that actually each point in synodical coordinates $(x, y, \dot{x}, \dot{y})$ have two associated points in Levi-Civita coordinates (u, v, u', v') and $(-u, -v, -u', -v')$. As $w_2 = \pm i$ and we only want an bijective change of variables, we only consider the upper plane in Levi-Civita coordinates (i.e. $v \geq 0$).

As we have seen in the previous proposition, the regularized equation is

$$w'' + 2i|f'|^2 w' = grad_w(U|f'|^2)$$

so we need to express U in terms of u and v.

$$\begin{aligned} U = \tilde{\Omega} - \frac{C}{2} &= \frac{1}{2}[(1-\mu)r_1^2 + \mu r_2^2] + \frac{1-\mu}{r_1} + \frac{\mu}{r_2} - \frac{C}{2} = \\ &= \frac{1}{2}[(1-\mu)|w|^4 + \mu|1+w^2|^2] + \frac{1-\mu}{|w|^2} + \frac{\mu}{|1+w^2|} - \frac{C}{2} = \\ &= \frac{1}{2}\Big[(1-\mu)(u^2+v^2)^2 + \mu[(u^2-v^2+1)^2 + 4u^2v^2]\Big] + \frac{1-\mu}{u^2+v^2} + \frac{\mu}{\sqrt{(u^2-v^2+1)^2+4u^2v^2}} - \frac{C}{2} \end{aligned}$$

because $r_1 = |w^2|$ and $r_2 = |1 + w^2|$. Hence, after handling properly the expressions, we get that

$$\begin{aligned} U|f'|^2 = 4U(u^2+v^2) = \\ = 2(u^2+v^2)^3 + 4\mu(u^4-v^4) + 2(\mu - C)(u^2+v^2) + \frac{4\mu(u^2+v^2)}{\sqrt{(u^2-v^2+1)^2+4u^2v^2}} + 4(1-\mu) \end{aligned}$$

Derivating this expression with respect to u and v, on one hand we get

$$(U|f'|^2)_u = 12u(u^2+v^2)^2 + 16\mu u^3 + 4(\mu - C)u + \frac{8\mu u(u^2-3v^2+1)}{((u^2-v^2+1)^2+4u^2v^2)^{3/2}}$$

while on the other hand we have

$$(U|f'|^2)_v = 12v(u^2+v^2)^2 - 16\mu v^3 + 4(\mu - C)v + \frac{8\mu v(3u^2-v^2+1)}{((u^2-v^2+1)^2+4u^2v^2)^{3/2}}$$

Because of these last two expressions, the only points where there exists a singularity are $w_2 = \pm i$, which correspond to the second primary and its symmetric point with respect to $\{v = 0\}$.

2.5.2 Regularization around $(\mu - 1, 0)$

On the other hand, if we focus now on the regularization around $(\mu - 1, 0)$, as we said we consider $z = f(w) = \mu - 1 + w^2$ and $\frac{dt}{ds} = 4(u^2+v^2)$, where $z = x + iy$ and $w = u + iv$. Hence we have

$$\begin{cases} x = \mu - 1 + u^2 - v^2 \\ y = 2uv \\ \dot{x} = \dfrac{uu' - vv'}{2(u^2+v^2)} \\ \dot{y} = \dfrac{uv' + vu'}{2(u^2+v^2)} \end{cases} \iff \begin{cases} u = \pm\sqrt{\dfrac{x-\mu+1+\sqrt{(x-\mu+1)^2+y^2}}{2}} \\ v = \pm\sqrt{-x+\mu-1+u^2} \\ u' = 2(\dot{x}u + \dot{y}v) \\ v' = 2(-\dot{x}v + \dot{y}u) \end{cases}$$

As in the previous case, we have two associated Levi-Civita points to each of the synodical ones. In this case we have $w_1 = \pm 1$, so we only consider $u \geq 0$ and as before we decide the sign of v depending on the sign of y. Using this change of variables, the new coordinates of the primaries and the origin point are

$$\begin{cases} z_1 = \mu \longrightarrow w_1 = \pm 1 \\ z_2 = \mu - 1 \longrightarrow w_2 = 0 \\ O_z = 0 \longrightarrow O_w = \pm\sqrt{\mu - 1} \end{cases}$$

As we have seen in the previous proposition, the regularized equation is

$$w'' + 2i|f'|^2 w' = grad_w(U|f'|^2)$$

so we need to express U in terms of u and v.

$$\begin{aligned} U = \tilde{\Omega} - \frac{C}{2} &= \frac{1}{2}[(1-\mu)r_1^2 + \mu r_2^2] + \frac{1-\mu}{r_1} + \frac{\mu}{r_2} - \frac{C}{2} = \\ &= \frac{1}{2}[(1-\mu)|w^2-1|^2 + \mu|w|^4] + \frac{1-\mu}{|w^2-1|} + \frac{\mu}{|w^2|} - \frac{C}{2} = \\ &= \frac{1}{2}\Big[(1-\mu)[(u^2-v^2-1)^2+4u^2v^2] + \mu(u^2+v^2)^2\Big] + \frac{1-\mu}{\sqrt{(u^2-v^2-1)^2+4u^2v^2}} + \frac{\mu}{u^2+v^2} - \frac{C}{2} \end{aligned}$$

because $r_1 = |w^2 - 1|$ and $r_2 = |w^2|$. Hence, after handling properly the expressions, we get that

$$U|f'|^2 = 4U(u^2+v^2) =$$
$$= 2(u^2+v^2)^3 - 4(1-\mu)(u^4-v^4) + 2(1-\mu-C)(u^2+v^2) + \frac{4(1-\mu)(u^2+v^2)}{\sqrt{(u^2-v^2-1)^2+4u^2v^2}} + 4\mu$$

Derivating this expression with respect to u and v, on one hand we get

$$(U|f'|^2)_u = 12u(u^2+v^2)^2 - 16(1-\mu)u^3 + 4(1-\mu-C)u + \frac{8(1-\mu)u(-u^2+3v^2+1)}{((u^2-v^2-1)^2+4u^2v^2)^{3/2}}$$

while on the other hand we have

$$(U|f'|^2)_v = 12v(u^2+v^2) + 16(1-\mu)v^3 + 4(1-\mu-C)v + \frac{8(1-\mu)v(-3u^2+v^2+1)}{((u^2-v^2-1)^2+4u^2v^2)^{3/2}}$$

Because of these last two expressions, the only points where there exists a singularity are $w_1 = \pm 1$, which correspond to the first primary and its symmetric point with respect to $\{u = 0\}$.

3 Periodic orbits around the equilibrium points

Our aim is to find a way to explain the behavior of the manifolds emanating from the periodic orbits around the equilibrium points. Even though we will do it by numerical inspection, it must have an analytic justification behind it. In this section we introduce the theorems and definitions related to the invariant manifolds, its existence and more particularly for our purpose, which are widely explained in Meyer, Hall and Offin [5] and in Stuart and Humphries [7]. As all of them are classical results, they are not proven in this project but they appear in many standard textbooks.

Definition 3.1. *Let $\dot{x} = f(x)$, with f smooth, be a system with an equilibrium point x^*. Then we call this equilibrium point elementary if all the exponents are non-zero.*

Definition 3.2. *Let $\dot{x} = f(x)$, with f smooth, be a system with a T-periodic solution $\phi_T(t, x^*)$. If the monodoromy matrix has 1 as eigenvalue of multiplicity one for the general case or multiplicity two if the system has a first integral then the periodic solution is called to be elementary.*

Theorem 3.1 (The cylinder theorem)**.** *An elementary periodic orbit of a system with a first integral that lies in a smooth cylinder of periodic solutions parameterized by the integral.*

This implies that the orbits around the equilibrium points will be paramaterized by the Jacobi integral. But before that we must prove the existence of these orbits. Taking the synodical equations of the RTBP, the differential matrix of the system is

$$Df = \begin{pmatrix} 0 & 0 & 1 & 0 \\ 0 & 0 & 0 & 1 \\ \Omega_{xx} & \Omega_{xy} & 0 & 2 \\ \Omega_{xy} & \Omega_{yy} & -2 & 0 \end{pmatrix}. \tag{3.1}$$

where

$$\begin{cases} \Omega_{xx} = 1 + (1-\mu)\dfrac{2(x-\mu)^2 - y^2}{r_1^5} + \mu\dfrac{2(x-\mu+1)^2 - y^2}{r_2^5} \\ \Omega_{xy} = 3y\left(\dfrac{(1-\mu)(x-\mu)}{r_1^5} + \dfrac{\mu(x-\mu+1)}{r_2^5}\right) \\ \Omega_{yy} = 1 + (1-\mu)\dfrac{2y^2 - (x-\mu)^2}{r_1^5} + \mu\dfrac{2y^2 - (x-\mu+1)^2}{r_2^5} \end{cases}$$

and the characteristic polynomial of Df is

$$p_c(\lambda) = \lambda^4 + (4 - \Omega_{xx} - \Omega_{yy})\lambda^2 + \Omega_{xx}\Omega_{yy} - \Omega_{xy}^2 = 0. \tag{3.2}$$

Focusing on the collinear equilibrium points, as $y = 0$ then we have

$$\begin{cases} \Omega_{xx}\big|_{y=0} = 1 + 2\left(\dfrac{1-\mu}{r_1^3} + \dfrac{\mu}{r_2^3}\right) > 0 \\ \Omega_{xy}\big|_{y=0} = 0 \\ \Omega_{yy}\big|_{y=0} = 1 - \dfrac{1-\mu}{r_1^3} - \dfrac{\mu}{r_2^3} < 0 \end{cases}$$

The first inequality is obvious as $r_1, r_2 \geq 0$ and the last one can be easily proved. As we have that $\Omega_x = x - \dfrac{(1-\mu)(x-\mu)}{r_1^3} - \dfrac{\mu(x-\mu+1)}{r_2^3}$, then restricted to $y=0$ we have $\Omega_x\big|_{y=0} = x - \dfrac{1-\mu}{r_1^2} - \dfrac{\mu}{r_2^2}$ and particularly for the equilibrium points as $\Omega_x\big|_{L_i} = 0$ they accomplish

$$\frac{1-\mu}{r_1^2} = x - \frac{\mu}{r_2^2}. \tag{3.3}$$

Now focusing on L_2, it accomplishes that $x = \mu - r_1$, so then the previous equation is equivalent to $\dfrac{1-\mu}{r_1^2} = -\mu + r_1 - \dfrac{\mu}{r_2^2}$. So eventually we get

$$\Omega_{yy}(L_2) = 1 - \frac{1}{r_1}\Big(r_1 - \mu - \frac{\mu}{r_2^2}\Big) - \frac{\mu}{r_2^3} \tag{3.4}$$

which after being simplified it can be expressed as

$$\Omega_{yy}(L_2) = \frac{\mu}{r_1}\Big(1 - \frac{1}{r_2^3}\Big). \tag{3.5}$$

As for L_2 we have $r_2 < 1$, hence it implies that $\Omega_{yy} < 0$. The cases of L_1 and L_3 can be proved using a similar procedure, so they will not be proven in this project as they do not introduce any interesting result.

Let us define $\beta_1 = 2 - \dfrac{\Omega_{xx} + \Omega_{yy}}{2}$ and $\beta_2^2 = -\Omega_{xx}\Omega_{yy} > 0$, then the roots of the characteristic polynomial evaluated at the collinear equilibrium points can be expressed as

$$p_c(\lambda) = \lambda^4 + 2\beta_1\lambda^2 - \beta_2^2 = 0 \tag{3.6}$$

and equivalently

$$\lambda^2 = -\beta_1 \pm \sqrt{\beta_1^2 + \beta_2^2}.$$

Hence the roots are $\lambda = \pm\alpha$ and $\lambda = \pm i\gamma$ with $\alpha, \gamma \in \mathbb{R}$, meaning that these equilibrium points are saddle-center. In order to prove that there exist symmetric periodic orbits around the equilibrium points, we may introduce Lyapunov Center Theorem.

Theorem 3.2 (Lyapunov Center Theorem)**.** *Let $\dot{x} = f(x)$, with f smooth, be a system with a first integral and an equilibrium point x^*, with characteristic exponents $\pm iw, \lambda_3, ..., \lambda_m$ where $iw \neq 0$ is pure imaginary and the exponents accomplish $\dfrac{\lambda_j}{iw} \notin \mathbb{Z}$ for $j = 3, ..., m$.*
Then, there exists a one parameter family of periodic orbits emanating from x^*. Furthermore, the period of these orbits tend to $\dfrac{2\pi}{w}$ when approaching to x^*.

Taking our equilibrium points, all of them accomplish the assumptions of the theorem and we consider the Jacobi integral as the integral mentioned, so around each of them there exists a one parameter family of periodic orbits which are elementary and parameterized by the Jacobi integral.

Let us consider the flow of the RTBP system $\phi_t(\boldsymbol{x})$, which is the point after integrating for time t with initial point $\boldsymbol{x}$. Hence, we know that for each point $\boldsymbol{x}_0$ of the T-periodic orbit around L_i it

accomplishes that $\phi_T(\boldsymbol{x}_0) = \boldsymbol{x}_0$, so all the points of the periodic orbit are fixed points of the map $\boldsymbol{x} \longrightarrow \phi_T(\boldsymbol{x})$. Actually it is true for any $t = mT$ where $m \in \mathbb{Z}$. In order to prove the existence of the manifolds of the periodic orbits, we introduce the following definition and theorems:

Definition 3.3. *For a linear map $x \longrightarrow Bx$ we define the stable and unstable subspaces as*

$$E^s = span\{n_s \text{ (generalized) eigenvectors whose eigenvalues have modulus } < 1\}$$

$$E^u = span\{n_u \text{ (generalized) eigenvectors whose eigenvalues have modulus } > 1\}$$

Definition 3.4. *Let us consider the map $G : \mathbb{R}^n \longrightarrow \mathbb{R}^n$ with an hyperbolic fixed point $\bar{x}$. Then we define its local stable and unstable manifolds as*

$$W^s_{loc} = \{x \in U | G^n(x) \longrightarrow \bar{x} \text{ as } n \longrightarrow \infty \text{ and } G^n(x) \in U \ \forall n \geq 0\}$$

$$W^u_{loc} = \{x \in U | G^{-n}(x) \longrightarrow \bar{x} \text{ as } n \longrightarrow \infty \text{ and } G^{-n}(x) \in U \ \forall n \geq 0\}$$

where U is a neighbourhood of $\bar{x}$.

Theorem 3.3 (Hartman-Grobman)**.** *Let $G : \mathbb{R}^n \longrightarrow \mathbb{R}^n$ be a (C^1) diffeomorphism with a hyperbolic fixed point $\bar{x}$. Then there exists a homeomorphism h defined on some neighbourhood U on $\bar{x}$ such that $h(G(\xi)) = DG(\bar{x})h(\xi)$ for all $\xi \in U$.*

Theorem 3.4 (Stable Manifold Theorem for a Fixed Point)**.** *Let $G : \mathbb{R}^n \longrightarrow \mathbb{R}^n$ be a (C^1) diffeomorphism with a hyperbolic fixed point $\bar{x}$. Then there are local stable and unstable manifolds $W^s_{loc}(\bar{x})$, $W^u_{loc}(\bar{x})$, tangent to the eigenspaces $E^s_{\bar{x}}$, $E^u_{\bar{x}}$ of $DG(\bar{x})$ at $\bar{x}$ and of corresponding dimensions. $W^s_{loc}(\bar{x})$ and $W^u_{loc}(\bar{x})$ are as smooth as the map G. Hence, we can define the global stable and unstable manifolds as*

$$W^s(\bar{x}) = \bigcup_{n \geq 0} G^{-n}(W^s_{loc}(\bar{x}))$$

$$W^u(\bar{x}) = \bigcup_{n \geq 0} G^{n}(W^u_{loc}(\bar{x})).$$

In our case, we are working with $G = \phi_T(\boldsymbol{x})$ so we have to compute the monodromy matrix at time T (which is the matrix DG of the theorem). It is known that the monodromy matrix of an ODE system with a first integral has a double multiplicity eigenvalue 1 (see Meyer, Hall and Offin[5]). As in the RTBP we have the Jacobi integral then the monodromy matrix will have two eigenvalues 1. Actually, the monodromy matrix of the RTBP has the set of eigenvalues $\{1, 1, 1/\lambda, \lambda\}$ with $\lambda > 1$. Hence, when restricting to C constant the significant eigenvalues are $1/\lambda$ and λ so we can apply the previous theorem because all the fixed point (points of the orbit) are hyperbolic. So finally we have proved that the stable and the unstable manifolds of the periodic orbits exist and we can start our study with the proper background.

4 Numerical simulations

The existence of symmetric periodic orbits around the collinear equilibrium points, which give rise to invariant manifolds from them, has been proved in the previous section from the theoretical point of view. Once we have reached this result, a natural continuation is to find them numerically. Hence, our goal in this section is to study the behavior of the invariant manifolds of these orbits around the collinear equilibrium points. We must take into account that it depends on the value of μ and the Jacobi integral associated to each orbit, so we must compare the behavior obtained in each case by varying these constants.

We can separate the stable manifold (W^s) and the unstable manifold (W^u) into two different branches which can be denoted as:

- $W_-^{u/s}$ a branch that tends (backward/forward) to the orbit from the lower half region $\{y < 0\}$.
- $W_+^{u/s}$ a branch that tends (backward/forward) to the orbit from the upper half region $\{y > 0\}$.

Despite the fact that there are four branches associated to each orbit we do not need to study the four of them because of the symmetry of the problem, see figure (4.1). So we will only focus on the behavior of W_+^u and W_-^u, which have the same interpretation that W_-^s and W_+^s, respectively.

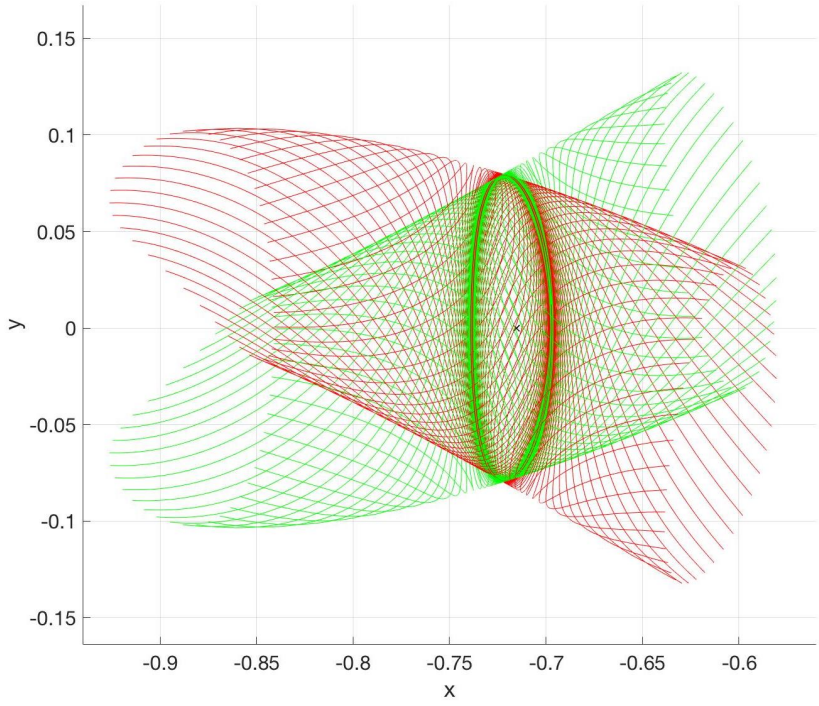

Figure 4.1: The Lyapunov periodic orbit (PO) and its stable (green) and unstable (red) branches of $W^{u,s}(PO)$, case of the orbit around L_1 for $\mu = 0.2$ and $C = C_2$. The symmetry is clearly seen in the picture.

4.1 Computation procedure

In order to avoid numerical problems due to the singularities of the problem, we use three different systems of coordinates which have been widely explained in the previous section:

- For points where $r_1, r_2 > \varepsilon$ we use synodical coordinates.
- For points where $r_1 \leq \varepsilon$ we use Levi-Civita coordinates around $(\mu, 0)$.
- For points where $r_2 \leq \varepsilon$ we use Levi-Civita coordinates around $(\mu - 1, 0)$.

where $\varepsilon > 0$ is the tolerance chosen (during our study we have used $\varepsilon = 10^{-3}$) and r_1 and r_2 are the distances to each primary using synodical coordinates. As it is more intuitive using synodical coordinates than Levi-Civita coordinates, we only use Levi-Civita when we are integrating close to one of the primaries but after having integrated we compute the equivalent points in synodical coordinates so all the points are expressed in these coordinates. This procedure is a key part of the project and must be clearly understood by the reader as it ensures that the whole study remains accurate and does not give false behaviors.

Although considering these change of coordinates avoids the singularities of the primaries, a very important issue is to keep the accuracy during the whole integration whichever are the coordinates we are using, so the best way is to check for every step of the integration if the Jacobi integral remains constant as it is an inherent property of the RTBP from the analytic point of view.

The procedure to compute the periodic orbits around the equilibrium points is nothing more than a problem of a zero of a function. We are looking for the symmetric orbit with respect to the x-axis in the (x, y) plane around L_i with Jacobi integral C, so actually we just need to find half of the orbit. Due to this symmetry, both the initial and the final points must accomplish $\dot{x} = 0$ and $y = 0$, which means that we cut perpendicularly $\{y = 0\}$ at $t = 0$ and $t = T/2$, where T is the period of the symmetric orbit. Using the initial value $x_0 > x_{L_i}$ then from the initial point $(x_0, 0, 0, \dot{y}_0)$, where $\dot{y}_0 = -\sqrt{2\Omega(x_0, 0) - C}$ because of the expression of the Jacobi integral and the retrograde movement of the orbit, we integrate until we cut $\{y = 0\}$ so we have the point $(x_f, 0, \dot{x}_f, \dot{y}_f)$. Hence, we are looking for a suitable initial value such that $\dot{x}_f = 0$ when $y = 0$, which is the perpendicularity condition, so it will provide an initial condition $(x_0, 0, 0, \dot{y}_0)$ of the symmetric periodic orbit.

It is very important to find the best approximation of the orbit, so the accuracy must be as precise as possible because it is the first step of the whole study. To do so, and in order to compute the family of periodic orbits, we start by finding the periodic associated with $C_i - \Delta C$, where C_i is the Jacobi integral at the point L_i and given ΔC. Once we have the suitable initial condition, we consider a new value $C_i - 2\Delta C$ and obtain the corresponding initial condition of the associated periodic orbit an so on. With this procedure we obtain a family of periodic orbits parametrized by C in a certain range of values C. In figure (4.2), we plot some periodic orbits around L_i, $i = 1, 2, 3$ for $\mu = 0.2$ and $C = C_i - 0.05k$, $k = 1, ..., 10$.

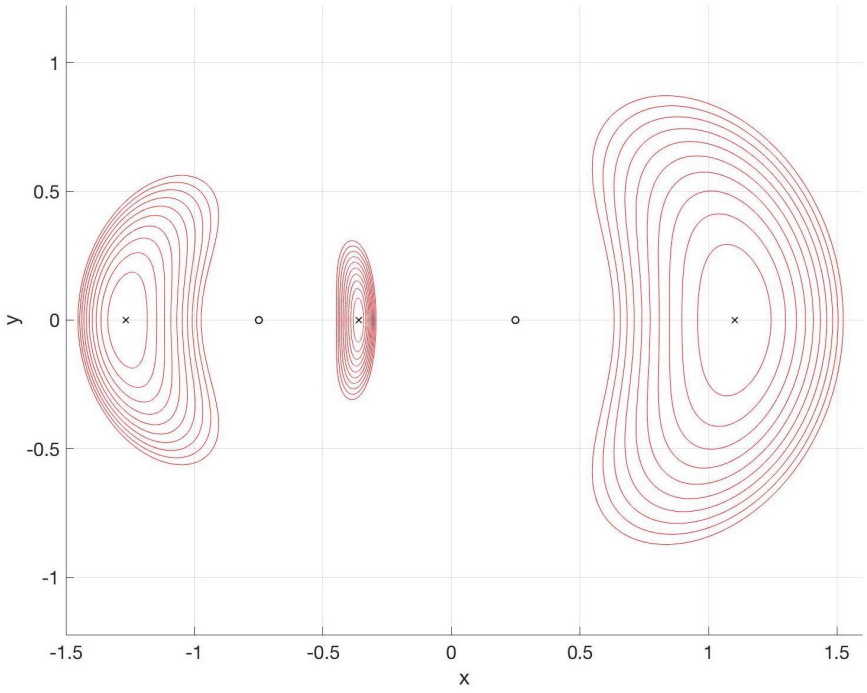

Figure 4.2: For $\mu = 0.2$ we take 10 symmetric orbits around the collinear equilibrium points with $C = C_i - k \cdot 0.05$ with $k = 1, \ldots, 10$.

Once we have the orbit around L_i we can start computing its invariant manifolds. Let us assume that $\boldsymbol{x}_0$ is a point of the orbit and T is the period of the orbit and by definition if we call the flow of the orbit as $\phi_t(\boldsymbol{x}_0)$, it accomplishes that $\phi_T(\boldsymbol{x}_0) = \boldsymbol{x}_0$. Here is important the role played by the variational equations of the system, which are

$$Y' = A(t)Y,\ Y(0) = Id \tag{4.1}$$

where $Y = D_{\boldsymbol{x}_0}\phi_t$ and the matrix $A(t)$ is

$$A(t) = \begin{pmatrix} 0 & 0 & 1 & 0 \\ 0 & 0 & 0 & 1 \\ \Omega_{xx} & \Omega_{xy} & 0 & 2 \\ \Omega_{xy} & \Omega_{yy} & -2 & 0 \end{pmatrix}.$$

For each point $\boldsymbol{x}_0$ of the orbit we integrate the variational equations and its trajectory both at the same time for $t \in [0, T]$ so we finally have the monodromy matrix $Y(T)$, which has the set of eigenvalues $\{\lambda, \frac{1}{\lambda}, 1, 1\}$ where $\lambda > 1$ and its eigenvectors give the direction of the perturbations that will give rise to the stable and the unstable manifold. The first eigenvalue is associated to the unstable manifold and the second one to the stable manifold, so let us call $\boldsymbol{v}_u$ and $\boldsymbol{v}_s$ the unitary eigenvectors associated to these eigenvalues and we take the orientation of the eigenvector such that the second coordinate of the vector is positive. Once we have these vectors we can compute

the invariant manifolds as follows: from a given point $\boldsymbol{p}$ of the periodic orbit, we take as initial condition of the associated orbit in the manifold $\boldsymbol{p} \pm s \cdot \boldsymbol{v}$ where $s = 10^{-6}$ and $\boldsymbol{v}$ is the eigenvector chosen depending on the manifold we want to compute and the sign refers to which branch of the manifold we want to study. Hence, in our case we take $\boldsymbol{p} + s \cdot \boldsymbol{v}_u$ for W^u_+ and $\boldsymbol{p} - s \cdot \boldsymbol{v}_u$ for W^u_-. Although this procedure can be done with any point of the orbit we only choose a finite number of initial conditions in the linear approximation of the manifold. A posteriori, we check that this approximation is good enough for our purpose. We integrate forward in time each initial condition giving rise to a trajectory on the corresponding branch W^u. Taking a finite set of initial conditions, we will obtain a finite set of trajectories on W^u.

4.2 Dynamical behavior of the invariant manifolds

In this section it has been described how to find the periodic orbits around the collinear equilibrium points from a general point of view so the procedure explained would be valid for any of the three collinear points. In this project we focus our attention on L_1 and consider the range of values $C \in [C_2, C_1)$. As we have seen in section 2, the manifolds of the orbit around L_1 are enclosed inside the area defined by the Hill's region of that level of C, which contains both primaries and L_1 but neither it contains L_2 (except for the case $C = C_2$ where L_2 belongs to the boundary of the region) nor L_3, so they will have no effect on the manifolds' behavior.

Let us fix a value of μ and a value of C. Let us consider the T-periodic orbit around L_1 and we call its initial point when we compute it as $\boldsymbol{x}_0 = (x_0, 0, 0, \dot{y}_0)$ with $x_0 > x_{L_1}$. Then each point $\tilde{\boldsymbol{x}}_0$ that belongs to the orbit will be identified with the number $\theta = \frac{\tilde{t}}{T} \in [0, 1]$ where $\tilde{t}$ is the time needed to reach $\tilde{\boldsymbol{x}}_0$ starting from $\boldsymbol{x}_0$. From now on we will refer to the value θ as the normalized time of the point $\tilde{\boldsymbol{x}}_0$.

A very important remark is that we parametrize the set of initial conditions of W^u_+ (or W^u_-) by θ in the sense that for each θ we consider the corresponding initial condition of the orbit on W^u as a perturbation perturbation of the point $\tilde{x}_0$, as explained above.

Once we have a periodic orbit around L_1, we want to study the behavior of the associated manifolds $W^{u,s}$. To do so, as we have already said, we will take a finite number of trajectories on W^u (by symmetry on W^s) so we take a finite number of points of the periodic orbit, and the corresponding suitable initial conditions of the orbits on W^u. We will integrate forward in time each orbit until we reach a certain condition.

In order to have a first intuition of the dynamics of the invariant manifolds, we compute W^u_- and W^u_+ up to the second cut with the sections $\{x = \mu\}$ and $\{x = \mu - 1\}$ respectively for different values of μ and C. In figure (4.3) we plot W^u_+ and W^u_- for particular values of μ and two specific values of the Jacobi integral $C = C_2$ and $C = (C_1 + C_2)/2$ and we notice that for these two levels of C the most remarkable difference is that for the smaller value of C the pipe created by the manifolds is wider than in the greater value case as the periodic orbit describes a bigger trajectory from L_1. On the other hand, when we vary the mass parameter μ we can see more important changes. When μ is small, because of the proximity of the small primary to L_1, W^u_+ gets really close to the primary while W^u_- stays further from the massive primary. Then, as μ increases the figures show us that W^u_+ gets further but W^u_- gets closer, basically because the distance to each primary increases and

decreases respectively. At first sight it may be surprising that for W^u_- we get closer to m_1 because for small values of μ there exists a huge difference of masses so we would expect that this manifold would tend much more to the massive body.

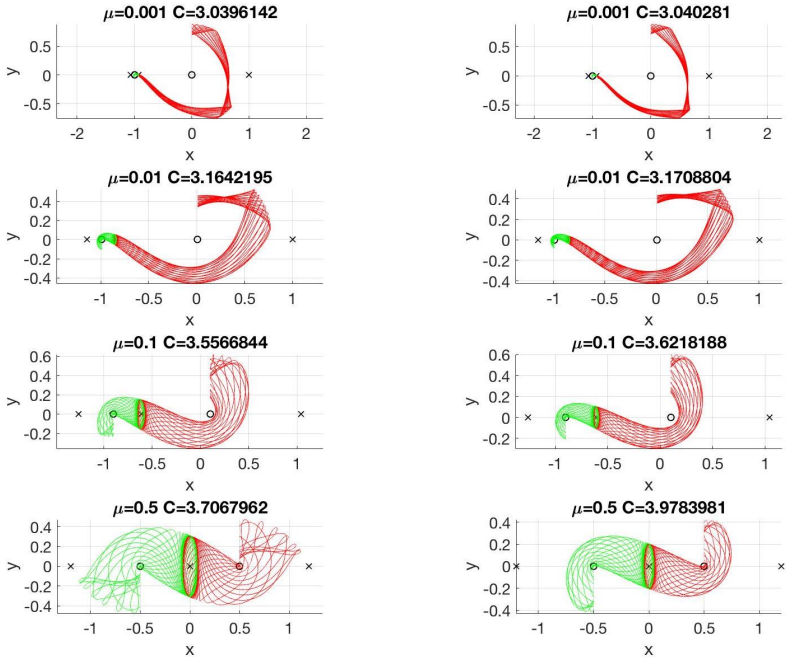

Figure 4.3: W^u_- (red) and W^u_+ (green) up to the second cut with sections $\{x = \mu\}$ and $\{x = \mu - 1\}$ respectively for different values of μ and $C = C_2$ (first column) or $C = (C_1 + C_2)/2$ (second column).

After having a first insight of the problem, let us consider the section minimum distance

$$\Sigma_{r_i} = \{\dot{r_i} = 0, \ddot{r_i} > 0\} \tag{4.2}$$

where r_i is the distance to the massive primary if $i = 1$ or the small primary if $i = 2$, depending on with respect to which body we want to study the distance. For each trajectory on W^u, we integrate forward in time up to the m-th cut with the section, so for each initial point of the orbit, identified by a number θ from 0 to 1 as explained before, we will have m points of minimum distance. Plotting θ versus the distance of the minimum then we will understand how each trajectory on W^u behaves and how close to the body it gets. Moreover, it would be interesting to detect the collisions with the primaries, so we consider the cross product

$$\boldsymbol{r}_i \times \dot{\boldsymbol{r}}_i \tag{4.3}$$

which will give us information about how the trajectory moves with respect to the primary when we cut the section Σ_{r_i}. We will overlap the plot of the distance and the cross product of the cuts with the section so when we have a distance really close to zero and the value of the cross product

cuts the x-axis, at that point there will exist a collision with the primary.

When we use the section Σ_{r_i} we have to take into account that we must distinguish which branch we are studying and with respect to which primary, so eventually we have four cases. Once we started to compute the intersection with Σ_{r_i} we noticed that we detected minimum distance points when the trajectories were still in a neighbourhood of the periodic orbit that caused discontinuity issues due to the fact that depending on the initial point of the orbit we detected a minimum near one of the intersections of the orbit with the x-axis or the other. Hence, we decided to create an initial region where we do not consider the minimum points of a trajectory until it has crossed the boundary of this region. Let us assume that x_{min} and x_{max} the minimum and the maximum value of the x-coordinates of the points of the orbit and y_{min} and y_{max} the minimum and maximum values of y. Then we define $\Delta x = x_{max} - x_{min}$ and $\Delta y = y_{max} - y_{min}$. Then we chose arbitrarily the initial region as $\{(x, y) \in \mathbb{R}^2 \mid x_{min} - \alpha\Delta x < x < x_{max} + \alpha\Delta x,\ y_{min} - \beta\Delta y < y < y_{max} + \alpha\Delta y\}$, where we have generally used $\alpha = \beta = 0.5$, although we must adapt these values to each case. In figure (4.4) we can see an example of the initial region where we have used $\alpha = 0.5$ and $\beta = 1$ for the case $\mu = 0.05$ and $C = C_2$.

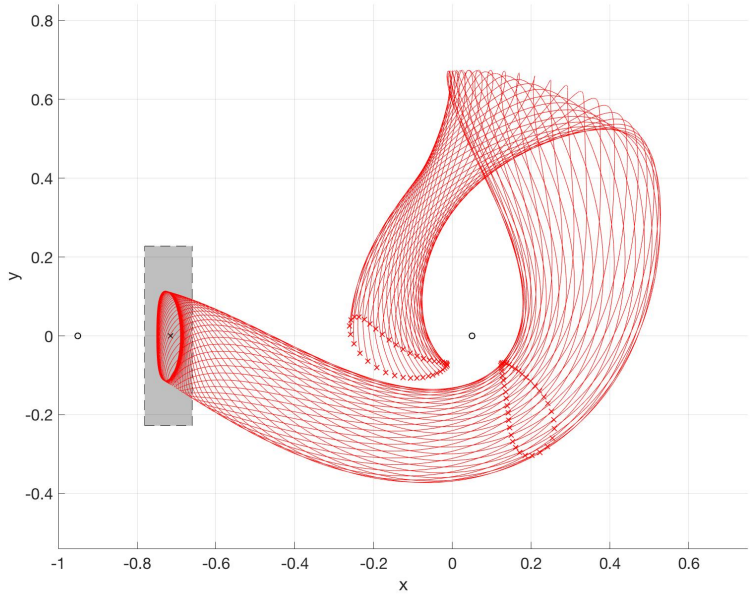

Figure 4.4: W^u_{-} up to the second cut with Σ_{r_1} for the case of $\mu = 0.05$ and $C = C_2$. The crosses locate the minimum distance points of each trajectory. The shaded area is the initial region where we do not gather the minimum distance points. In this case we have used $\alpha = 0.5$ and $\beta = 1$.

Once we have all the previous considerations stated we can start to compute the invariant manifolds, considering the plots up to the first cut with Σ_{r_i}. As W^u_{-} is pointing to m_1, we consider the first intersection with Σ_{r_1} for $C = C_2$ and $C = (C_1 + C_2)/2$ for different values of μ.

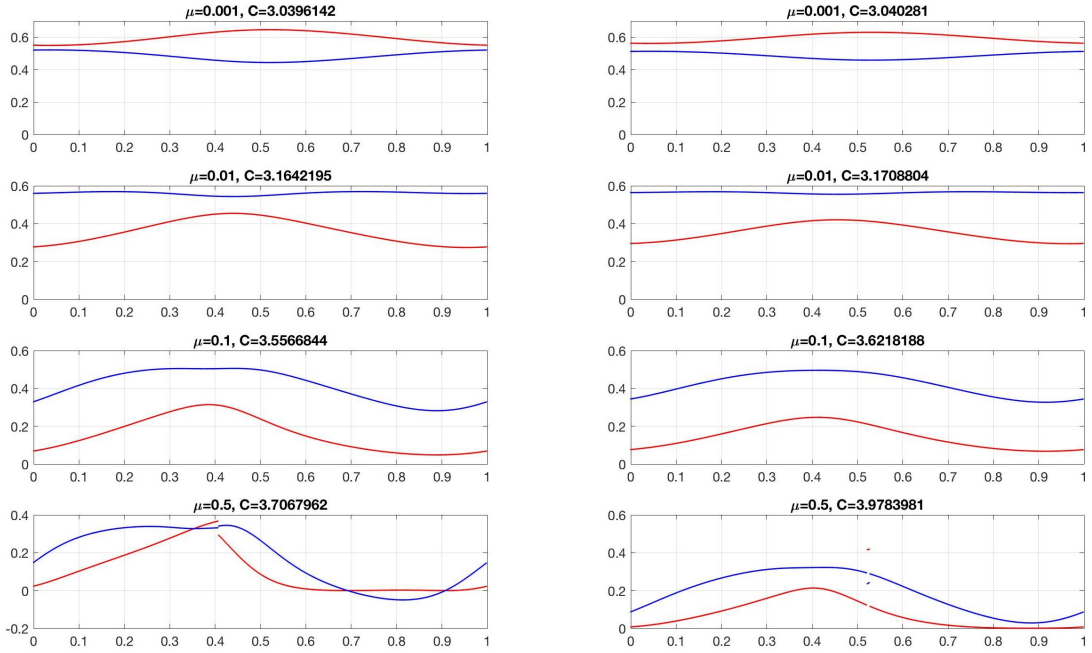

Figure 4.5: First intersection of W^u_- with Σ_{r_1}. We overlap r_1 (red) with the cross product $\boldsymbol{r}_1 \times \dot{\boldsymbol{r}}_1$ (blue) for different values of μ. The first column refers to $C = C_2$ and the second one to $C = (C_1 + C_2)/2$.

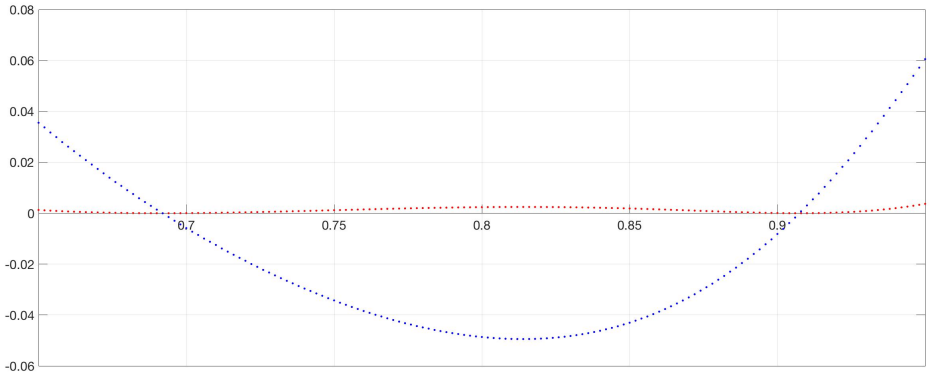

Figure 4.6: Zoom of the first intersection of W^u_- with Σ_{r_1}, $\mu = 0.5$ and $C = C_2$. We appreciate collisions with m_1 for $\theta_1 \approx 0.692$ and $\theta_2 \approx 0.907$. We plot r_1 (red) and the cross product $\boldsymbol{r}_1 \times \dot{\boldsymbol{r}}_1$ (blue).

As we see in the figure (4.5), it follows the behavior seen in figure (4.3), where as μ increases we get closer to m_1. Furthermore, $\mu = 0.5$ is the only value where the difference between the two levels of C is remarkable because for $C = C_2$ we detect two collisions at normalized time $\theta_1 \approx 0.692$

and $\theta_2 \approx 0.907$ as the function $\boldsymbol{r}_1 \times \dot{\boldsymbol{r}}_1$ crosses the x-axis and the distance function is numerically 0, as it can be seen in figure (4.6).

An important fact that we start to notice in this figure is that for $\mu = 0.5$ there appear jump discontinuities for both levels of C. The discontinuity of $C = C_2$ is produced at normalized time $\theta \approx 0.407$ and the discontinuity of $C = (C_1 + C_2)/2$ is produced for a small interval of normalized time $\theta \in [0.522, 0.526]$. These discontinuities will be explained later in this section with more details.

On the other hand we consider W_+^u with respect to m_2 using Σ_{r_2}. As figure (4.7) shows, there is not a significant difference on the general behavior of the manifold when varying C apart from the fact that we have collisions for $C = C_2$. We detect four different collisions with m_2, two of them for $\mu = 0.1$ and the other two for $\mu = 0.5$ while for the other value of C we have not detected any collision for these cases at the first minimum distance.

The main difference obtained has been when varying μ. For the smallest values we see that all the minimum distance points are quite close to m_2 while for greater μ there are points which get further from it but other ranges of points get so close that there even exist collisions for the two greater values studied.

It is also remarkable the discontinuity found for $\mu = 0.1$ and $C = C_2$, which is equivalent to the ones of $\mu = 0.5$ and $C = (C_1 + C_2)/2$. As before, it will be explained later for another particular case. In addition, we must notice that the graphics for $\mu = 0.5$ are like the ones obtained for W_-^u but with a translation on the normalized time value of 0.5 (meaning half orbit), which is quite obvious due to the fact that both primaries have the same mass so their attraction is equal.

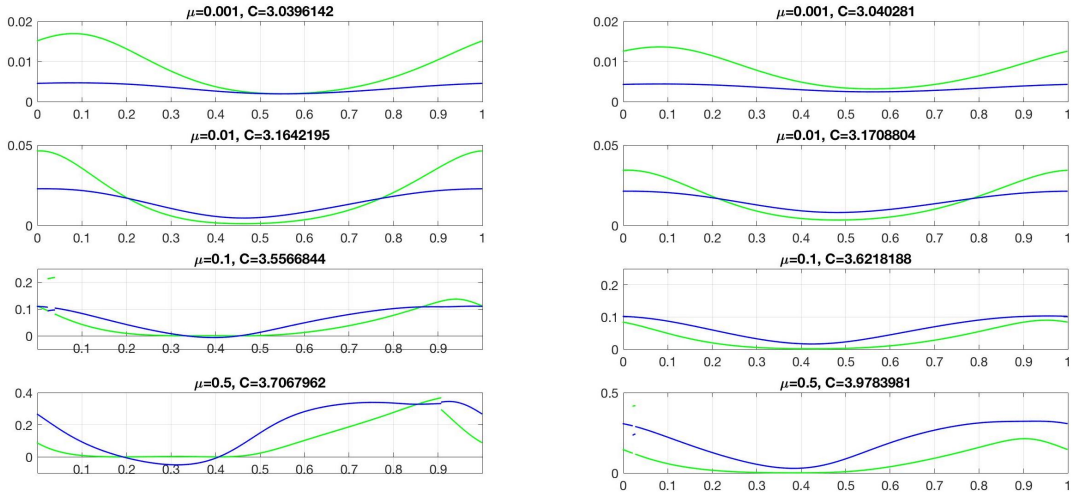

Figure 4.7: First intersection of W_+^u with Σ_{r_2}. We overlap r_2 (green) with the cross product $\boldsymbol{r}_2 \times \dot{\boldsymbol{r}}_2$ (blue) for different values of μ. The first column refers to $C = C_2$ and the second one to $C = (C_1 + C_2)/2$.

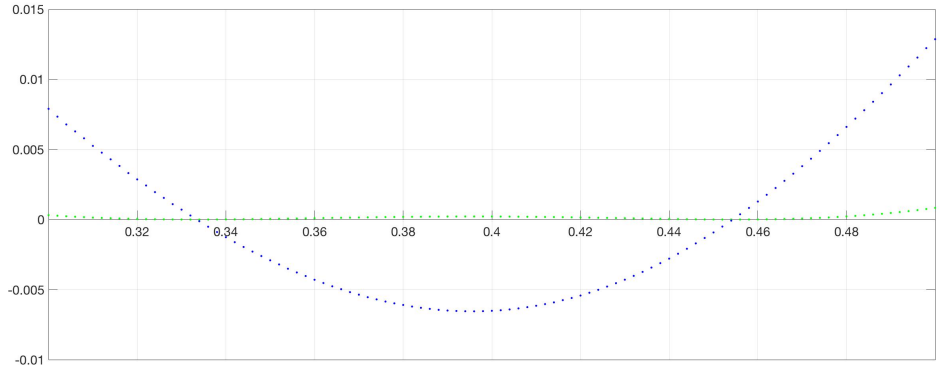

Figure 4.8: Zoom for the first intersection of W_+^u with Σ_{r_2}, $\mu = 0.1$ and $C = C_2$. Collisions with m_2 for $\theta_1 \approx 0.333$ and $\theta_2 \approx 0.455$. We plot r_2 (green) and the cross product $\boldsymbol{r}_2 \times \dot{\boldsymbol{r}}_2$ (blue).

In figure (4.8) we see the collisions with m_2 for the case $\mu = 0.1$ and $C = C_2$. The collisions of the case $\mu = 0.5$ and $C = C_2$ are not plotted because they are equivalent to the ones seen in the other branch of the manifold as we have explained before.

On the other hand, we can consider the second cuts of these manifolds with each section. As we can see in the figures (4.9) and (4.10), in the second cut there start to appear important discontinuities issues which have to be studied one by one and does not let us study properly the general behavior of the manifolds. Also due to these discontinuities, it is quite difficult to interpret the cross product $\boldsymbol{r}_i \times \dot{\boldsymbol{r}}_i$ overlapped with the distance to the primary, so in these cases we will not plot it.

In figures (4.9) and (4.10), specially in the second one, we see a lot of discontinuities. In part because of them, we appreciate that some of the distance values are close to 1 or even greater than it, so we suspect that maybe these trajectories have escaped to the other primary. When doing this justification we must take into account the shape of Hill's region for $C = C_2$ as it can be seen in figure (2.15). Thanks to this property of the RTBP we can claim that if the trajectory is at distance 1 or greater, it must be close to the other primary.

Except for the case $\mu = 0.5$, the invariant manifold W_-^u keeps almost the same distances with respect to m_1 than for the first intersection. Actually for small values of μ this manifold keeps rotating around m_1 for much greater number of intersections, which is justified by the more important attraction caused by the massive primary with mass $m_1 = 1 - \mu$. On the other hand the invariant manifold W_+^u does not behave so well, appearing much more issues than for the other branch, justified again by the difference of masses between both primaries which causes that m_1 has more attraction than m_2.

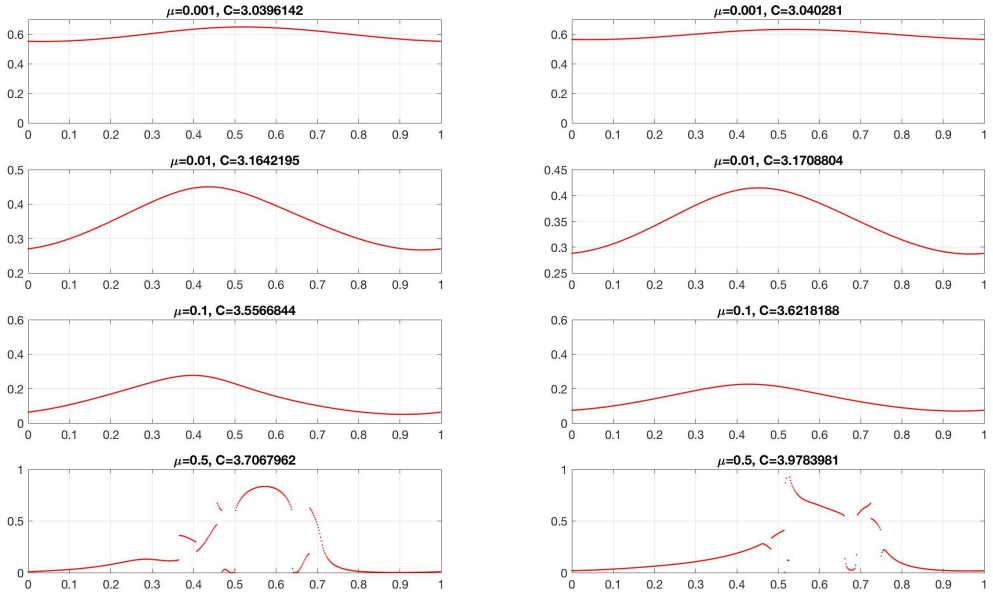

Figure 4.9: Distance of W^u_- to m_1 at the second cut with Σ_{r_1}. The first column refers to $C = C_2$ and the second one to $C = (C_1 + C_2)/2$.

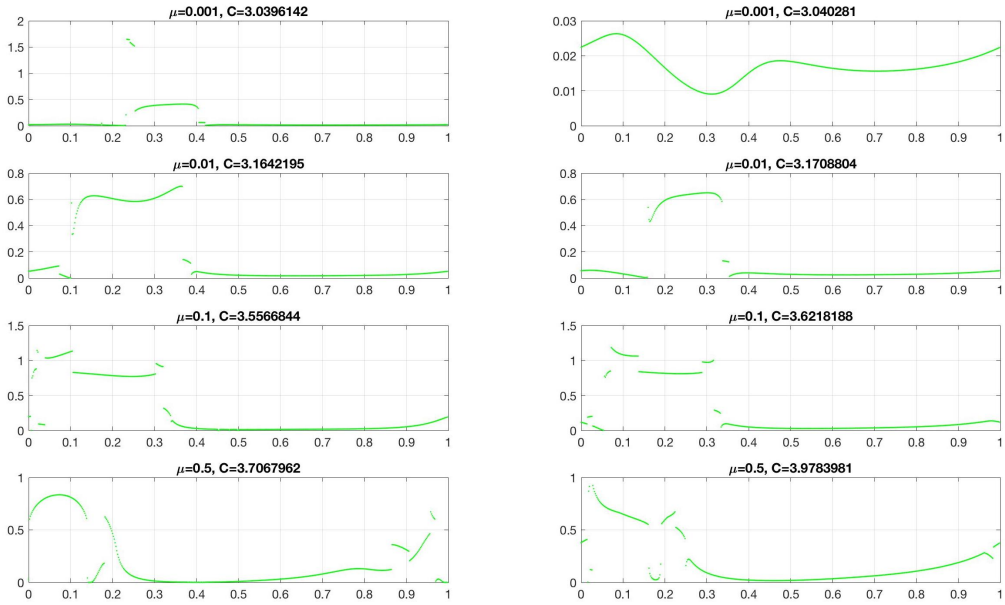

Figure 4.10: Distance of W^u_+ to m_2 at the second cut with Σ_{r_2}. The first column refers to $C = C_2$ and the second one to $C = (C_1 + C_2)/2$.

Let us focus on the crossed cases where we consider W^u_- with respect to m_2 and W^u_+ with respect to m_1. As we are trying to find the minimum distance points with respect to the primary where we are not pointing there appear discontinuities on the first cut with the minimum distance section as we can find trajectories that initially go to the primary where they are pointing and then tend to the other primary before finding the first minimum distance point while other really close points of the orbit start its trajectory and stay near the primary where they are pointing.

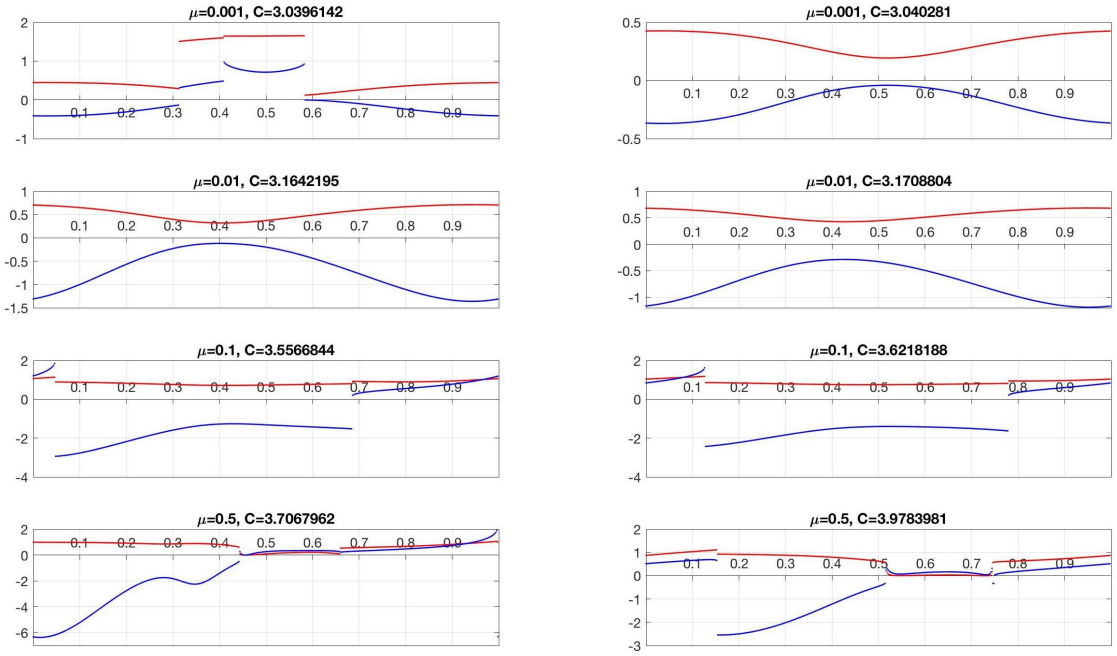

Figure 4.11: First intersection of W^u_- with Σ_{r_2}. We overlap r_1 (red) with the cross product $\boldsymbol{r} \times \dot{\boldsymbol{r}}$ (blue) for different values of μ. The first column refers to $C = C_2$ and the second one to $C = (C_1 + C_2)/2$.

Figure 4.12: Zoom for the first intersection of W^u_- with Σ_{r_2} for $\mu = 0.5$. We overlap r_1 (red) with the cross product $\boldsymbol{r} \times \dot{\boldsymbol{r}}$ (blue) for different values of μ. We appreciate two collisions for $C = C_2$ at normalized time $\theta_1 \approx 0.451$ and $\theta_2 \approx 0.458$. The case $C = (C_1 + C_2)/2$ does not show collisions.

As we see in figure (4.11) we do not detect any collision with the primary for the three first values of μ as we are studying W^u_- with respect to m_2 but we detect some discontinuities that will be studied deeper later. Although the first three values of μ does not give us much more information than what we already knew, the last one gives us a surprising behavior as for both values of values

we detect an interval of values of normalized time such that the branch gets very close to m_2 while the other ones stay further. In addition we see in figure (4.6) that actually we detect two collisions with the primary for normalized time $\theta_1 \approx 0.951$ and $\theta_2 \approx 0.958$ for $\mu = 0.5$ and $C = C_2$ while for the case where $C = (C_1 + C_2)/2$ we do not detect any collisions.

Comparing it with the results given by figure (4.9), we see that these same interval of values where we see discontinuities for the first cut of W^u_- with the section Σ_{r_2} are the same ones that gave us discontinuities for the second cut with section Σ_{r_1}.

On the other hand, considering the other crossed case where we study W^u_+ with respect to m_1, we see again some intervals of discontinuities in figure (4.13) because of the same fact than in the previous case. In addition we don't detect any collision for the three first cases but for the last one, because of the symmetry of the case $\mu = 0.5$ between both branches, we can use the same reasoning to justify that there exist two collisions with m_1 for $C = C_2$ for $\theta_1 \approx 0.951$ and $\theta_2 \approx 0.958$ and for $C = (C_1 + C_2)/2$ we do not detect any collision.

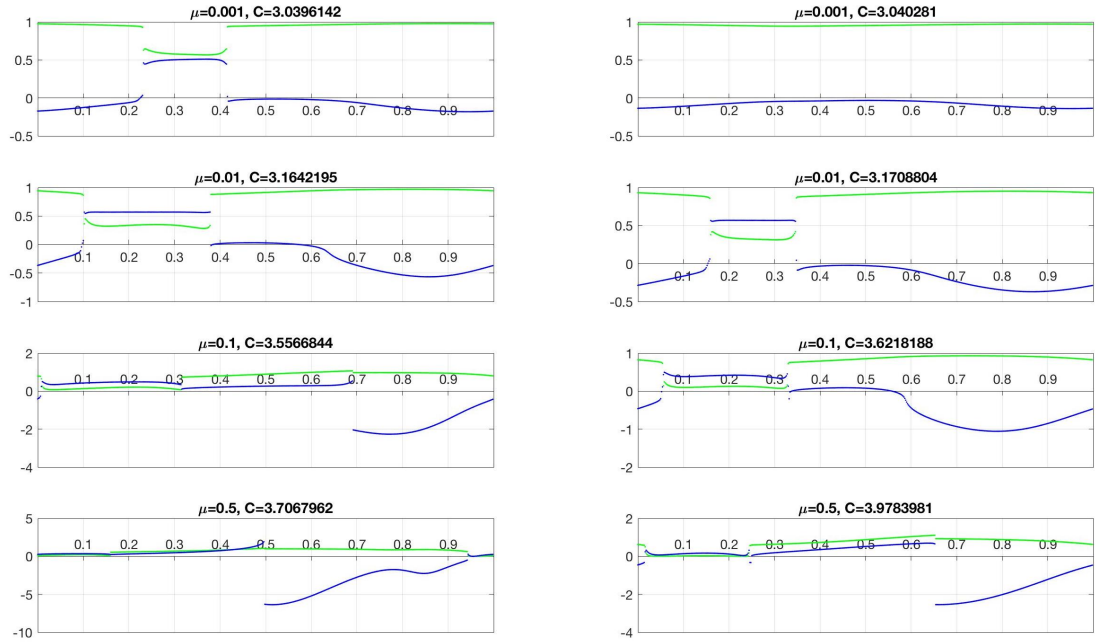

Figure 4.13: First intersection of W^u_+ with Σ_{r_1}. We overlap r_2 (green) with the cross product $\boldsymbol{r} \times \dot{\boldsymbol{r}}$ (blue) for different values of μ. The first column refers to $C = C_2$ and the second one to $C = (C_1 + C_2)/2$.

In the previous figures we have only considered up to the first or the second cut with the section because for greater number of cuts there were too many discontinuities so we couldn't do a good general comparison between the different cases. Although the discontinuities may seem like an error of the procedure or something bad, they hide a very rich and useful meaning behind them. After studying all the cases we have found three different types of discontinuities:

1. Problems with the initial region
2. Homoclinic trajectories
3. Detection of progressive minimums

The first case is basically the one that we can see in figures (4.5) and (4.7) for $\mu = 0.5$ and $C = C_2$. There appears a jump discontinuity because the first minimum points of the trajectories tend to the boundary of the initial area when varying the initial point associated and then we reach an interval of values which have the first minimum inside the region so we do not detect it even though by continuity it exists. Hence, whichever initial region we decided we could not avoid this discontinuity neither for Σ_{r_1} nor for Σ_{r_2}. As we can see in figure (4.14) where the minimum distance points (marked with crosses) tend to the initial region until there is a value where the minimum is inside the region so we do not consider it.

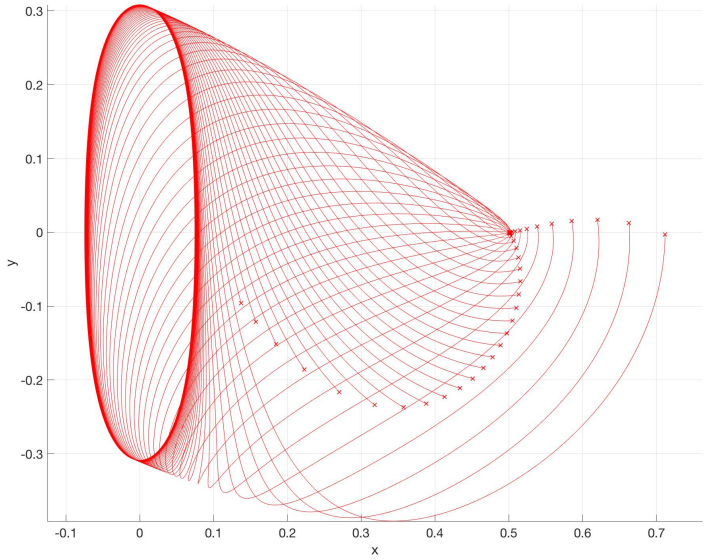

Figure 4.14: Projection on the (x, y) plane of W^u_- up to the first cut with Σ_{r_1} for $\mu = 0.5$ and $C = C_2$. The crosses mark when the minimum distance is detected.

Let us focus now on $\mu = 0.01215$, which is the mass parameter of the system Earth-Moon, and $C = C_2$ in order to explain the different discontinuities with a real case which makes it more interesting. Although from now on we will study this particular case, this procedure could be done with other cases because after having done inspections with different values of μ and C, the discontinuities found have the same behavior as the ones of the Earth-Moon system, so we will explain them for this particular one.

As we have seen, the branch W^u_- has a very good behavior when μ is small, so for this particular case we have inspected up to the fourth cross with Σ_{r_1} and the behavior seen is quite uniform

giving a very well defined shape of the invariant manifold when plotted as we can see in figure (4.15) and without having neither any discontinuity of the distance function nor any collision with the primaries for the first four intersections.

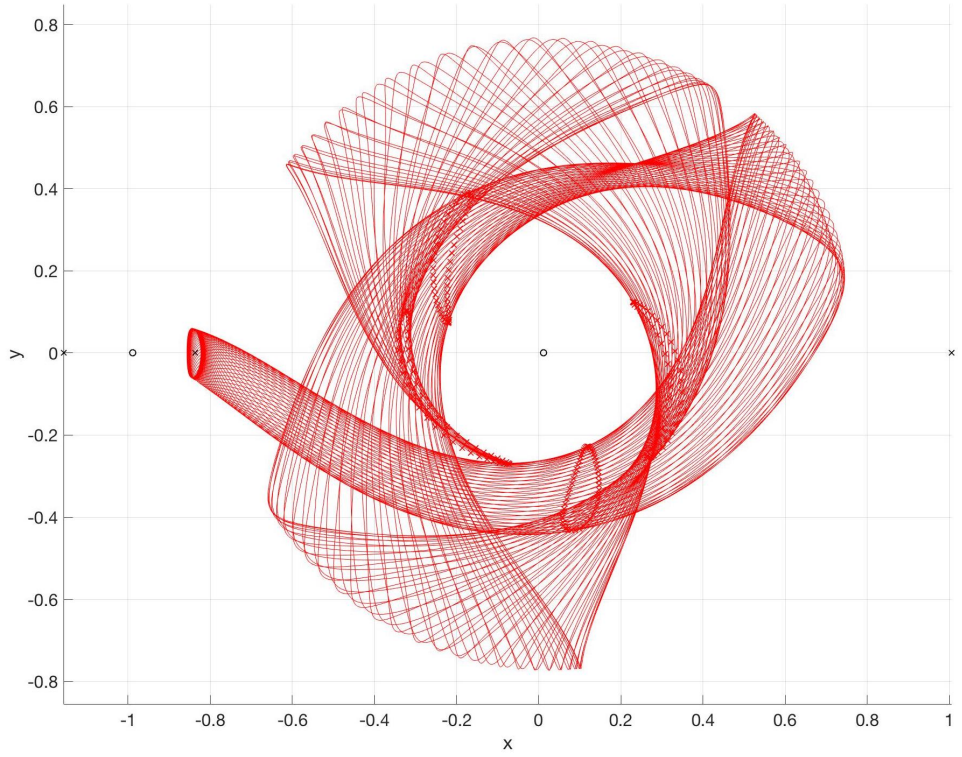

Figure 4.15: Projection on the (x, y) plane of W_+^u up to the fourth intersection with Σ_{r_1}. The crosses mark where the minimum distance points of each trajectory are produced.

The second type of discontinuities that we have mentioned is the case where there exists a point belonging to the orbit such that its associated trajectory ends up again in the initial orbit. Let us consider W_-^u up to the second cut with the section Σ_{r_2}. This is one of the crossed minimum detection which give rise to discontinuities even at the first intersection for certain μ values.

Focusing on W_+^u with respect to m_2 and considering up to the second intersection we get the figure (4.16) plots we can see the second type of discontinuity. Taking a small interval of the normalized time in a neighbourhood of $\theta = 0.092$ we realize that after the first minimum distance with m_2, which in some cases is quite close as we can notice, some trajectories get close to the initial orbit and some of them go back to m_2 but other ones scape to the other primary, but between them by continuity we can assure that there exists a trajectory such that after the first minimum point we go back the initial orbit.

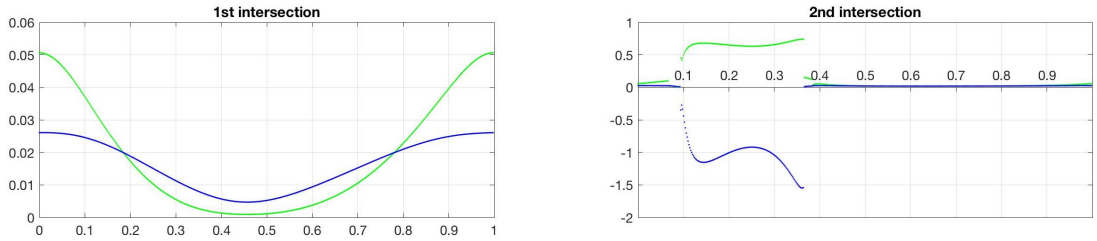

Figure 4.16: W^u_+ first (left) and second (right) intersections with Σ_{r_2}. Overlapped r_2 (green) and $\boldsymbol{r_2} \times \dot{\boldsymbol{r}}_{\boldsymbol{2}}$ (blue). Case of $\mu = 0.01215$ and $C = C_2$.

In figure (4.17) we can appreciate that the trajectory associated to $\theta = 0.092631$ after getting really close to the initial orbit, it goes back close to m_2 while the one associated to $\theta = 0.092637$ does not stay but it goes to m_1. Although the second trajectory finally escapes, we see a certain tendency to follow the shape of the initial periodic orbit around L_1. Hence, by continuity it must exist a value $\theta \in (0.092631, 0.092637)$ such that it creates an homoclinic orbit.

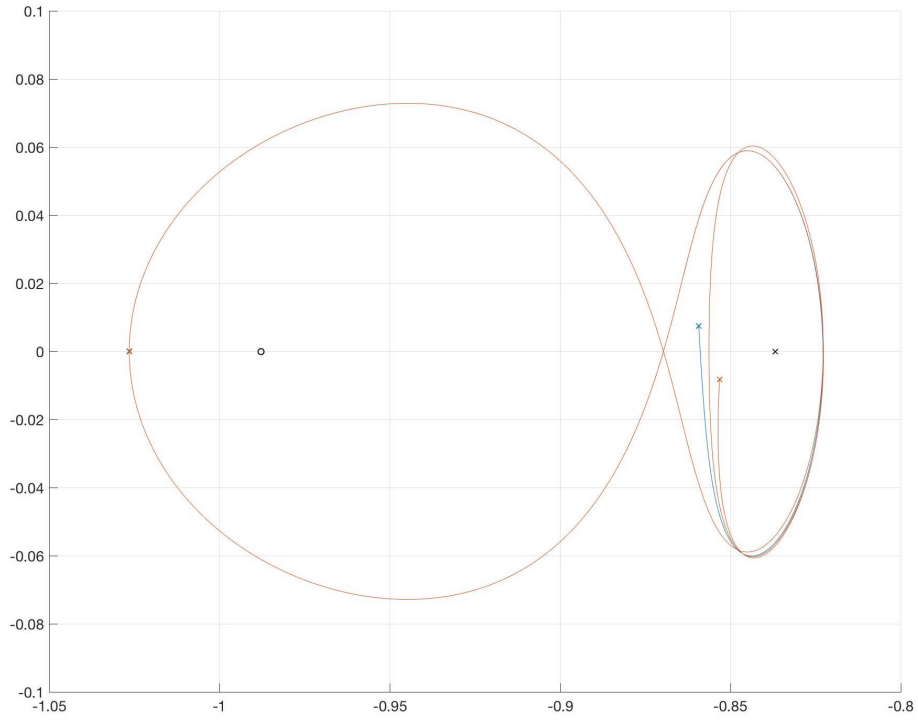

Figure 4.17: Projection on the (x, y) plane of the trajectories of $\theta_1 = 0.092631$ (blue) and $\theta_2 = 0.092637$ (orange) for the case $\mu = 0.01215$ and $C = C_2$. We take up to the second intersection of W^u_+ with Σ_{r_2}.

Finally, we refer to the third type of discontinuities as progressive minimums. We call them this way because we mean that there exists a range of points of the orbit that reach a minimum

distance with respect to either of the primaries but other close to this interval does not detect it. These phenomenon creates a jump discontinuity on the graphic of the distance, but plotting the graphic of the $\dot{r}_i$ against the time for a small group of points belonging to a neighbourhood of the one associated to the discontinuity we can understand why do we detect a minimum only for a group of points, as we can see in figure (4.20).

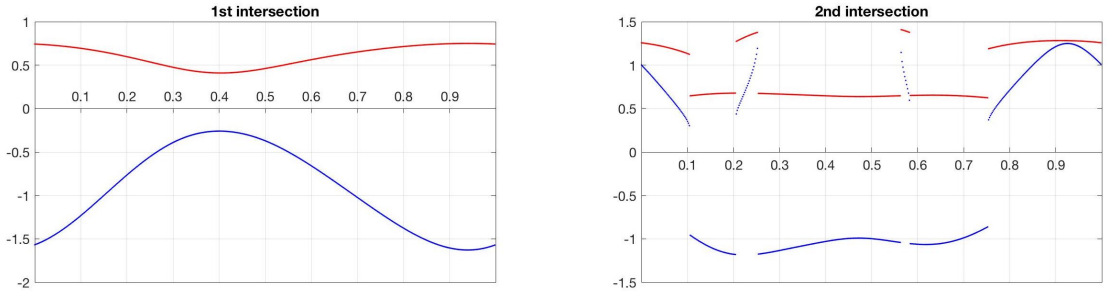

Figure 4.18: W^u_- first (left) and second (right) intersections with Σ_{r_2}. Overlapped r_2 (red) and $\boldsymbol{r_2} \times \dot{\boldsymbol{r}}_{\boldsymbol{2}}$ (blue). Case of $\mu = 0.01215$ and $C = C_2$.

The discontinuity produced at $\theta \approx 0.105$ at the right hand side of the figure (4.18) is quite clear that for smaller values (such as $\theta = 0.104$) we detect the second minimum distance point much sooner than for greater ones (such as $\theta = 0.106$). In order to understand it we can take a look to figure (4.20) where the function $\dot{r}_2$ associated to $\theta = 0.104$ crosses the x-axis producing a minimum point while the other trajectory clearly does not reach a minimum. We must notice that the minimum distance points are produced when we cross the x-axis from the region $\{\dot{r}_i < 0\}$ to $\{\dot{r}_i > 0\}$ as in this case we will have $\ddot{r}_i > 0$, otherwise we reach a maximum distance point.

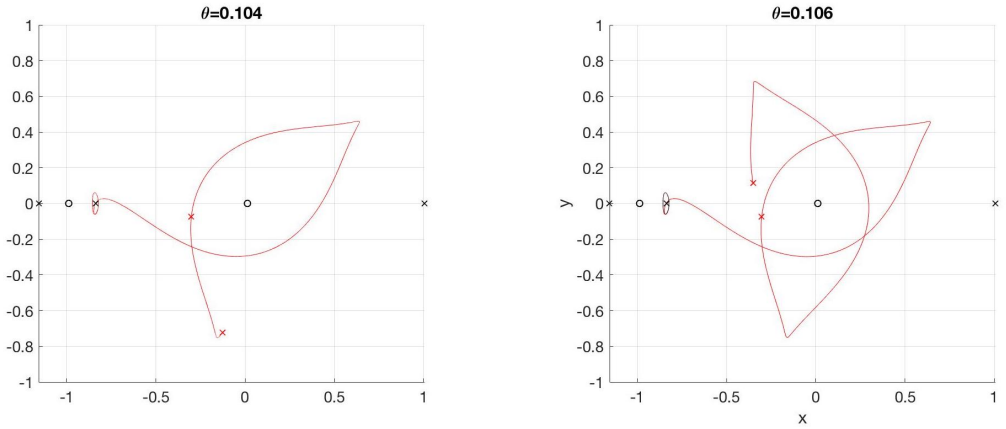

Figure 4.19: Trajectores of the points associated to $\theta = 0.104$ (left) and $\theta = 0.106$ (right) taking the W^u_- branch up to the second cut with section Σ_{r_2}. Marked with crosses the minimum distance points to m_2.

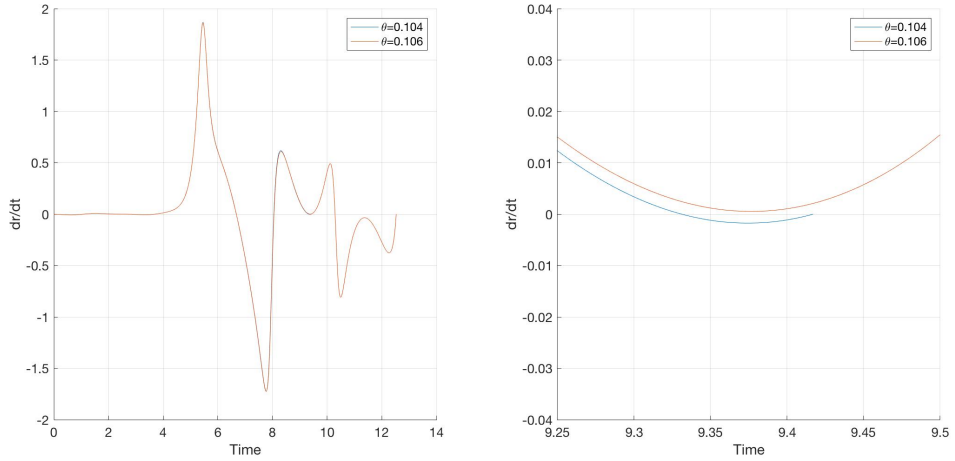

Figure 4.20: Representation of the function $\dot{r}_2$ with respect with time for the initial points associated to $\theta = 0.104$ (blue) and $\theta = 0.106$ (orange) of W^u_- for $\mu = 0.01215$ and $C = C_2$. Complete evaluation up to the second minimum distance point (left) and zoom of the function at the reason of the discontinuity (right).

This behavior is intrinsic to the manifolds' dynamics and it is impossible to avoid, so we must take into account that when studying the RTBP with section Σ_{r_i} there can appear these type of discontinuities. All the other discontinuities of the second intersection of the figure (4.18) are due to the same fact.

In spite the only way to assure the kind of discontinuity given a plot of the distance to a primary is to explore it numerically, after having done a lot of inspections we detect a certain tendency that enable us to distinguish them. If we face discontinuity such that at the edges of the distance function is quite vertical then we are most probably facing a discontinuity due to an homoclinic trajectory. In this case, if we could take an infinite number of points we wouldn't find this discontinuity but as we are using numerical methods it is not possible so we see it as a discontinuity. In case that we have a discontinuity where the edges of the interval change does not create this vertical shape, then we will face a case of a progressive minimum or a problem with the initial region. In case that the discontinuity is found at the first cut then we will need to inspect it numerically to decide but if it is for a greater number of cuts then it will be for sure a progressive minimum point. It is important to keep in mind that once we have a discontinuity for a certain value θ then all the following cuts with the section will show a discontinuity at that value.

5 Conclusions

Despite the fact that this project is mainly numerical, it has been necessary to do a deep study of the theoretical background related to the RTBP as all the following procedures and results rely on it, specially important has been the research and work devoted to Levi-Civita regularization because they avoid having singularities which would have caused that our study was not reliable at all. On the other hand, once we proved the existence of the periodic orbits and their manifolds we could start computing them numerically.

The main core of the project has been the one devoted to the numerical study of the problem. We developed a method to compute the orbits around each of the collinear equilibrium points and their manfolds, so we could continue this project in the future considering a more general case where we could take the orbits around L_2 and L_3. Our main goal was to describe the dynamics of $W^{u,s}$ of the periodic orbits around L_1, so we spent a lot of time and energy trying to find the best way to describe them graphically. We worked with different sections in order to study the invariant manifolds, such as $\{y = 0\}$, $\{x = \mu\}$ and $\{x = \mu - 1\}$, and after trying to understand all the difficulties and taking into account which of them give us more information we decided that the minimum distance was the one that fitted the best with our purpose. The section Σ_{r_i} has the discontinuities as an inherent property, so we had to adapt to this fact. Thanks to the study of this section and its discontinuities we have seen collisions with both primaries, homoclinic trajectories that emanate from the orbit and return to it and the progressive minimums, being able to distinguish between the discontinuities graphically almost for any case.

Once we have studied all the different cases, we have found out that a general study of the case is quite hard to do because when we increase the number of cuts with the section the discontinuities also increase because if a discontinuity appears at the m-th cut, then for all the greater cuts it will appear too. Hence the analysis of the results are quite complicated to compare between the different values of μ and C used, so this study might be better done case by case studying each of them separately so we can discard in each case the discontinuities found and follow the behavior of the manifold comparing the results found with Σ_{r_1} and Σ_{r_2}.

This project has been quite challenging for me, on one hand because of the conceptual difficulty of the project itself but particularly because it meant to me a big change of mind on how to face this problem. During the degree we are used to working with a clear path to follow when doing an exam, a project or any kind of exercise as we usually follow the guide and tips of the professor who previously has worked on the case and exactly knows what happens, then more or less we know what results we can expect. In this project we had a clear goal, but not a clear path, we have worked on the strategy to reach it, we found unexpected problems which surprised us and we solved them by trying other ways to overcome the situation or taking them with a different perspective so this issue could become a great result, as it happened with the discontinuities found during our study. Hence, although the Final Degree Project has given to me knowledge and experience dealing with the RTBP and the manipulation of numerical procedures, I think that the richest part of the project has been the one related to learn how to organize, to have the capacity of rethinking the strategy and how to overcome any difficulty appeared during our work. So finally, step by step, we leave the academic way of work and we face the real world.

6 References

[1] Barrabés, E., Mondelo, J.M., Ollé, M. : *Dynamical aspects of multi-round horseshoe-shaped homoclinic orbits in the RTBP*. Celest. Mech. Dyn. Astr. (2009) 105:197–210.

[2] Davis, K.E., Anderson, R.L., Scheeres, D.J., Born, G.H.: *The use of invariant manifolds for transfers between unstable periodic orbits of different energies*, Celest. Mech. Dyn. Astr. (2010) 107:471–485.

[3] Gómez, G., Mondelo, J.M.: *The dynamics around the collinear equilibrium points of the RTBP*.

[4] Guckenheimer, J., Holmes, P.J.: *Nonlinear oscillations, dynamical systems and bifurcations of vector fields*, Springer Science (1983).

[5] Meyer, K.R., Hall, G.R., Offin, D.: *Introduction to Hamiltonian Systems and the N-Body Problem*, Springer Science (2009).

[6] Murison, M.A.: *On an efficient and accurate method to integrate Restricted Three-Body orbits*, The Astronomical Journal, Volume 97, Number 5 (1989).

[7] Stuart, A.M., Humphries, A.R.: *Dynamical Systems and Numerical Analysis*, Cambridge University Press (1998).

[8] Szebehely, V.: *Theory of orbits*, Academic Press Inc., New York (1967)

7 Appendix

For this project, it has been necessary to create programs using Matlab in order to do any necessary computation. All the scripts can be found in the following link on GitHub:
https://gist.github.com/adriatorrentcanelles/68770a55b2e41884b5f8d9b74c296dc0.

The main scripts are main.m and main_plots_explicatius.m where most of the computations illustrated in this project are gathered.